SANDIA REPORT

SAND2009-0692
Unlimited Release
Printed February, 2009

Small Space Object Imaging: LDRD Final Report

Michael T. Valley, Sean P. Kearney, and Mark Ackermann

Prepared by
Sandia National Laboratories
Albuquerque, New Mexico 87185 and Livermore, California 94550

Sandia is a multiprogram laboratory operated by Sandia Corporation,
a Lockheed Martin Company, for the United States Department of Energy's
National Nuclear Security Administration under Contract DE-AC04-94AL85000.

Issued by Sandia National Laboratories, operated for the United States Department of Energy by Sandia Corporation.

Available to DOE and DOE contractors from
U.S. Department of Energy
Office of Scientific and Technical Information
P.O. Box 62
Oak Ridge, TN 37831

Telephone: (865)576-8401
Facsimile: (865)576-5728
E-Mail: reports@adonis.osti.gov
Online ordering: http://www.osti.gov/bridge

Available to the public from
U.S. Department of Commerce
National Technical Information Service
5285 Port Royal Rd
Springfield, VA 22161

Telephone: (800)553-6847
Facsimile: (703)605-6900
E-Mail: orders@ntis.fedworld.gov
Online order: http://www.ntis.gov/help/ordermethods.asp?loc=7-4-0#online

SAND2009-0692
Unlimited Release
Printed October 2009

Small Space Object Imaging: LDRD Final Report

Michael T. Valley and Sean P. Kearney
Thermal/Fluid Experimental Sciences Department 1512

Mark R. Ackermann
Emerging Threats Department 5928

Sandia National Laboratories
P.O. Box 5800
Albuquerque, NM 87185-0826

Abstract

We report the results of an LDRD effort to investigate new technologies for the identification of small-sized (mm to cm) debris in low-earth orbit. This small-yet-energetic debris presents a threat to the integrity of space-assets worldwide and represents significant security challenge to the international community. We present a nonexhaustive review of recent US and Russian efforts to meet the challenges of debris identification and removal and then provide a detailed description of joint US-Russian plans for sensitive, laser-based imaging of small debris at distances of hundreds of kilometers and relative velocities of several kilometers per second. Plans for the upcoming experimental testing of these imaging schemes are presented and a preliminary path toward system integration is identified.

Table of Contents

Executive Summary **1**

Introduction and Problem Overview **2**

Background **3**

Imaging Concepts **4**
Sample US Space Object Imaging Development Programs 4
Sample Russian Space Object Imaging Development Programs 9
SAPSAN Imaging Concept 10
SAPSAN Imaging System Design 13

Application of highly sensitive nonlinear optical methods for imaging space debris **19**
Space Object Illumination Operating Concept 20
Application of phase conjugation methods for concentrating the illumination of space debris 21
Technical Challenges 23
Illumination Laser Options 24
Test Plan Options 25
BEFWM Lab Test Scheme 25
Test Plan for One-pass Aberration Correction by BEFWM 29

Conclusions **33**

List of Figures

Figure 1: Optical layout of 3.0-deg prime focus corrector for the Discovery Channel Telescope. 6
Figure 2: Optical performance of 3.0 deg PFC for Discovery Channel Telescope. Ray-traced analysis indicates spots less than 1-arcsec diameter 7
Figure 3: Detection threshold for 600mm telescope as function of target angular rate. Integration time is shown on the x-axis while visual magnitude is shown on the y-axis..... 8
Figure 4: Photograph of the main meeting participants pictures at the entrance to the ranging and imaging telescope radome at the Altai Laser Optical site..... 10
Figure 5: Atmospheric absorption losses (star magnitudes) encountered during space object imaging at different zenith distances for two cases: a) p = 0.8 – normal transparency of atmosphere; b) p=0.7 – visible haze in atmosphere..... 12
Figure 6: Attenuation of space object integral brightness as a function of the phase angle in terms of star magnitudes 13
Figure 7: Mutual position of fields of view of 2 «Sapsan-200» and 2 «Sapsan-125» lenses. The system with the larger field of view would have a sensitivity of 9m and the sensitivity of the system with the smaller field of view is 13m 15
Figure 8: System diagram illustrating the illumination concentration channel and the detailed imaging channel using either sunlight or laser illumination 16
Figure 9: Diagram of the secondary flex mirror for the informational lens system «SAPSAN-1000»..... 17
Figure 10: Sapsan system rendering 18
Figure 11: System schematic. IL – illumination laser; LA – laser amplifier; MO – master oscillator; BEFWM – Brillouin Enhanced Four-Wave-Mixing system 20
Figure 12: IPG fiber laser for illumination of space objects..... 25
Figure 13: Proposed optical arrangement for testing of BEFWM concept for small object imaging 26
Figure 14: Schematic of two-pulse master oscillator for target illumination and BEFWM pump beams 26
Figure 15: Target area layout for planned BEFWM experiments 28
Figure 16: BEFWM image amplifier. Here: 1- input lens; 2 - laser amplifier; 3 - PC-mirror lens; 4 - PC-mirror via BEFWM; 5 - beam-splitting mirror; A - object plane; B - image plane..... 30
Figure 17: Idea of possible scheme modification for one-pass aberration correction. Here: 1-input lens; 2 - laser amplifier; 3 - PC-mirror lens; 4 - PC-mirror via BEFWM; 5 - beam-splitting mirror; 6 - retro-reflector; A - object plane; B - image plane 31
Figure 18: Modified BEFWM scheme for one-pass aberration correction 32

List of Tables

Table 1: Integral brightness of space object in the visible band (star magnitudes)…….11

Table 2: SAPSAN imaging system characteristics…….....14

Table 3: Minimal illumination energy for space debris observation by BEFWM image amplifier without concentration……..22

Table 4: Minimum space-debris-illumination energy at one-step and two-step concentration…22

Executive Summary

Space debris is a growing international challenge that remains unsolved. Many debris removal concepts have been proposed but they have proven to be impractical or non-viable. One promising technique studied in the USAF Orion program involved the potential use of lasers to de-orbit debris. Though the required laser technology exists, the Orion study confirmed that no method exists to image small debris, which renders the basic concept of laser removal unusable. However, progress in advanced imaging methods may make the development of ground-to-space imaging for space debris removal more viable.

This report documents the findings from a brief investigation of Russian and US imaging concepts including debris search and detection considerations. The optical systems considered include the DARPA space surveillance telescope, the Discovery Channel Telescope (DCT), a modified DCT telescope, and the Russian Sapsan telescope proposal. Additionally, this report discusses the viability of nonlinear laser-based methods (e.g., Brillouin enhanced four-wave mixing laser illuminator combined with Stimulated Brillouin Scattering optical amplifier) for detecting, imaging, characterizing, and tracking small space objects (i.e., 1 mm to 30 cm) such as debris and micro-satellites in the presence of atmospheric turbulence and intervening particles such as those present in the exo-atmospheric debris clouds. A full understanding of this area will set the stage for the development of state-of-the-art ground to space high-resolution imaging capabilities for tracking and imaging objects in LEO to GEO altitudes and advanced approaches for mitigating turbulence degradation of space-object images.

Introduction and Problem Overview

Space debris constitutes an increasing international danger to ground, air and space activities. Since the start of the space era on October 4, 1957, more than 4,400 launches have occurred and about 200 major fragmentations and numerous release events have taken place resulting in approximately 650,000 objects sized between 1 and 10 cm in low-earth orbit. The number of tracked space objects in the US Space Surveillance Network (SSN) catalog is about 13,000 now, corresponding to an estimated 5,000 tons of debris. The quantity of non-catalogued debris is far larger with approximately 650,000 objects sized between 1 and 10 cm. [1] Debris fragments larger than 1 cm will penetrate and damage most spacecraft, jeopardizing operations and potentially increasing the volume of debris through cascade events as ejected debris subsequently leads to more impacts and progressively larger volumes of orbital debris. Indeed, energy from a typical 10-cm fragment is roughly comparable to the explosive energy of 25 sticks of dynamite. Further, the growing volume of debris clouds with small fragments is creating an increasing likelihood of disruptions to communications, both ground-to-space and space-to-space. Current international efforts focus on minimizing the growth in debris and navigating through debris rather than small debris detection and removal. Though the UN has international debris mitigation guidelines, countries such as China and Ukraine do not honor these conventions. Consider, for example, that on January 11, 2007, as part of an anti-satellite test, China flew a kinetic energy interceptor into its own Fengyun 1C weather satellite. By year's end, 2,500 pieces of debris from this intercept were being tracked and it is estimated that approximately 35,000 pieces of debris down to 1 cm in size were created. It is estimated that this event increased the debris population in LEO by 10% and doubled the trackable objects at 800 km. [2] Last summer one of those Chinese satellite fragments forced NASA to hastily move its $1.3 billion Terra Earth-viewing spacecraft to avoid a collision. These kinds of evasive maneuvers are no longer uncommon for large spacecraft, including the International Space Station. Unfortunately, as pointed out by Dr. Nicholas Johnson, NASA Chief Scientist for Orbital Debris, if all launch activity were halted today, space debris levels would remain constant for about 50 years and then increase as existing pieces of orbital junk collide or explode into still more pieces. [3] Further, it is estimated that after 100 years only 17% of the debris from the Chinese intercept will have deorbited. [2] Hence, the proliferation of potentially hazardous orbital junk is a problem that will worsen particularly as more countries enter space.

Orbital debris generally has high relative velocities. In LEO (altitudes lower than 2,000 km) the average relative velocity at impact is about 8.0-10.0 km/s. At this velocity small particles contain significant amounts of kinetic energy and momentum. For example, NASA frequently replaces space shuttle orbiter windows because they are significantly damaged by objects as small as a flake of paint. An aluminum sphere of 1.3 mm in diameter has damage potential similar to that of a 22-caliber long rifle bullet. An aluminum sphere of 1 cm in diameter is comparable to a 160-kg safe moving at 100 km per hour. Energy from a 10-cm-long fragment is roughly comparable to the explosion energy of 25 sticks of dynamite. Debris fragments between 1 and 10 cm in size will penetrate and damage most spacecraft, jeopardizing operations and potentially increasing the volume of debris through cascade events as many smaller objects produce orbital debris, which in turn increases the overall risk to objects in orbit.

Space debris is a global problem and must involve an international effort. Sandia is well-positioned to take a leadership role in addressing this important challenge. It is recognized that no one project can redress this problem, nor is it economically practical to shield each spacecraft

and give it maneuvering capabilities. However, as stated in a Space News editorial report: "With so much at stake, research into affordable means of orbital-debris removal – studies have suggested that ground-based lasers might be able to do the job – should be accorded a higher priority by all space faring nations. Given what is known about the threat today, there can be little excuse for waiting until there is a catastrophic collision involving an operational spacecraft."[3] Though various studies and publications have discussed this problem and potential solutions, many challenges remain to be solved. [4-7]

Background

In 1995-96 the USAF Space Command and NASA commissioned a study called Orion to consider the viability of a laser debris removal system. [8] According to Nicholas Johnson, NASA Chief Scientist for Orbital Debris, Orion "turned out to be not all that easy technically". [9] The most difficult aspect in the ORION concept was acquiring, imaging, and tracking objects as small as 1 cm at ranges up to 1500 km since current space surveillance cameras track objects only down to 10 centimeters. Given the lack of required imaging capabilities, the Orion study proposed a laser debris-removal system that would not rely on debris detection, identification, or tracking (i.e., fire into a fixed volume of space to remove all debris that flies through the irradiated zone). The Orion project concluded that the concept of using ground-based lasers for removing orbital debris is feasible and cost effective relative to the cost of placing objects in orbit, but the concept of firing a laser at targets that were not resolvable was considered unacceptable. The need for ground-to-space imaging capabilities still exists.

Currently, tracking 10-cm objects requires very specialized radar capabilities such as the US COBRA Dane Space Surveillance Network phased array radar located in Shemya, AK or the Haystack X-Band radar site in Massachusetts (NASA's main source of data for debris smaller than 30 cm). Debris and space-object tracking over 10 cm is tracked by US Space Command (USSPACECOM), using 25 land-based radars and optical telescopes in the Space Surveillance Network, though they can only track the motion, not image the very small objects. For example, a 10-30 cm object will create a streak on an image during the camera or radar system data acquisition window, distinguishing it from a stationary star that creates a bright spot. However, this streak does not provide a resolved image of the object. Hence, to field viable options for detecting small space object (and to mitigate debris), one must first solve the long-standing challenge of developing an imaging capability to identify and characterize debris and other small space objects, particularly in the range of 1 mm to 30 cm. According to the US Space Command SSN website, "the SSN tracks space objects which are 10 centimeters in diameter (baseball size) or larger. The SSN uses a "predictive" technique to monitor space objects, i.e., it spot checks them rather than tracking them continually. This technique is used because of the limits of the SSN (number of sensors, geographic distribution, capability, and availability)."

Beyond Orion, many other alternatives have been considered for removing orbital debris, but no technically feasible or cost effective solutions have been developed. These schemes have included space flypapers, sweepers, robot garbage scows, a propeller-like sweeper (U.S. patent no. 4,991,799), and a robot that could grab space junk with "inflatable fingers." (patent no. 6,655,637), the US Terminator Tether developed by Tethers Unlimited, and the US Orbital Recovery Corporation ConeXpress Life. [3] In most instances, these and related ideas were outlandish or cost prohibitive, leaving the need for a viable space-debris-removal technology.

Optical methods are the main source of information for high-orbit space objects. These methods provide for search, detection and tracking of the objects as well as for obtaining coordinate and photometric characteristics, though they must rely on sunlight illumination (not suitable for day-night use) and are subject to atmospheric degradation. This study investigated emerging alternatives for providing the desired imaging capabilities, including the preliminary evaluation of a laser-based phase-conjugation approach for providing the desired imaging capabilities. The atmosphere degrades imagery and has two major effects on a laser beam: scintillation, which causes incoherence and spreading of the beam, and nonlinear effects, which spread the beam in wavelength, spatially, or both. The chief nonlinear effects come from atmospheric turbulence, absorption, dirty air breakdown, stimulated Raman scattering, thermal blooming, stimulated thermal Rayleigh scattering, and nonlinear refractive index. A phase-conjugation approach based on Brillouin-enhanced four-wave mixing may be viable for turbulence mitigation and target illumination if it is combined with Stimulated-Brillouin-Scattering and optical amplifiers to overcome low target light levels, thereby providing high resolution (1-10 cm) imaging and allowing the use of lower intensity illumination lasers that avoid some of these nonlinear optical issues.

Imaging Concepts

The principal existing methods to find, detect, track, and identify small space objects image the object's own or reflected electromagnetic radiation [1] and typically rely on:

a. Optical telescopes
b. Phased array radars
c. Spacecraft with optical and radar capabilities

Radars are primarily used for low-orbit space monitoring. Optical methods are the main source of information on high-orbit space objects. These methods provide for search, detection and tracking of the objects as well as for obtaining coordinate and photometric characteristics. Although the need exists to track all man-made orbital objects, technological and natural constraints limit the effective tracking of objects smaller than 10 cm and limit the accurate identification/imaging of objects below 50 cm. In recent years this has led to inadvertent collisions between orbital space objects. Though collisions with debris are the principal concern, some countries are experimenting with micro-satellites, which because of their small size are difficult to track and catalog. Further, when considering potential space debris removal systems it is important to reliably distinguish between space debris and micro-satellites to preclude the inadvertent removal of a micro-satellite.

This report considers space object imaging concepts under development in the United States and in Russia. Though not comprehensive, this report highlights a few notable programs and potential options for further testing and development.

Sample US Space Object Imaging Development Programs

Imaging distant space objects is an important part of space situational awareness (SSA), but it is impossible to image that which you cannot first detect, and second track. Radar systems are traditionally used to detect and track objects in low earth orbits (LEO), but have insufficient

power for higher altitudes, and rapid changes in range rate for objects in intermediate transfer orbits cause them to pass through Doppler bins too fast for effective detection and tracking.

Optical systems are traditionally used for space objects in high orbits where they are almost always solar illuminated. Some attempts are underway to explore the utility of optical systems for detection and tracking at low altitudes, but in general, objects move so fast that optical systems are ill-suited to this mission. Nonetheless, radar systems represent very large, fixed, high-dollar assets and are not suitable for locating all around the world. Optical systems by contrast are orders of magnitude less expensive, relatively small and can be made transportable if necessary.

Space debris represents a particularly interesting and important class of space object. At LEO altitudes, debris is considerable and represents a significant problem. Most such debris is too small to give an effective radar return and hence, much of the existing space debris is not tracked or characterized. This might be an interesting application of optical detection and tracking systems if effective methods of detection through a blind (un-cued) search can be devised.

At present, the Defense Advanced Research Projects Agency (DARPA) is in the final stages of developing a new space surveillance telescope (SST). This system is a proof-of-concept unit and includes many new technologies and aims to provide a significant improvement in capability for optical detection and tracking, but like its predecessors, is intended mostly for high altitude. The SST does include some capability for monitoring objects in transfer orbits as well.

The DARPA SST (DSST) will have a 3.5m aperture and 3.5deg field of view. An interesting feature of the DSST is that it will image a rectangle roughly 2 × 2.95 degrees, inscribed within its 3.5-deg light circle. The most important measure of a telescope's ability to search the sky for dim space debris is the system etendue (throughput). This is simply the product of effective aperture and effective field of view. On the surface, the DSST should have an etendue of roughly 92.5m^2deg^2, but when one includes geometric obscuration of the optics, this drops to 59.3 m^2deg^2, and with the optical transmission included, this drops further to only 49.3 m^2deg^2, and finally when the area of the actual detector is figured in, this drops to a value of only 30.2 m^2deg^2, roughly one third the initial value.

At a cost somewhere in excess of $65M, the value of the DSST is a fair target for questions. Comparison with a simple project being run by civilian astronomers at the Lowell Observatory in Arizona, the Discovery Channel Telescope (DCT) will have a 4.2m aperture and feature a prime focus corrector with a 2.0 deg field of view. At a cost of only $35M, this appears on the surface to be an interesting alternative to the DSST. The raw etendue for the DCT is only 43.5 m^2deg^2, but as the DCT uses a much simpler optical design than the DSST, with geometric optics, this value drops to only 32.6m^2deg^2, and with telescope transmission, it drops to 29.2m^2deg^2. The DCT can use a hexagonal pattern for imaging and tiling the sky, thereby using a higher percentage of the available light circle than the DSST. With geometric tiling losses of the focal plane array included, the DCT etendue drops to 24.5m^2deg^2, giving it roughly 84% of the raw search capability of the DSST for slightly over 50% of the cost. Clearly two DCT systems could greatly exceed the DSST for roughly the same cost.

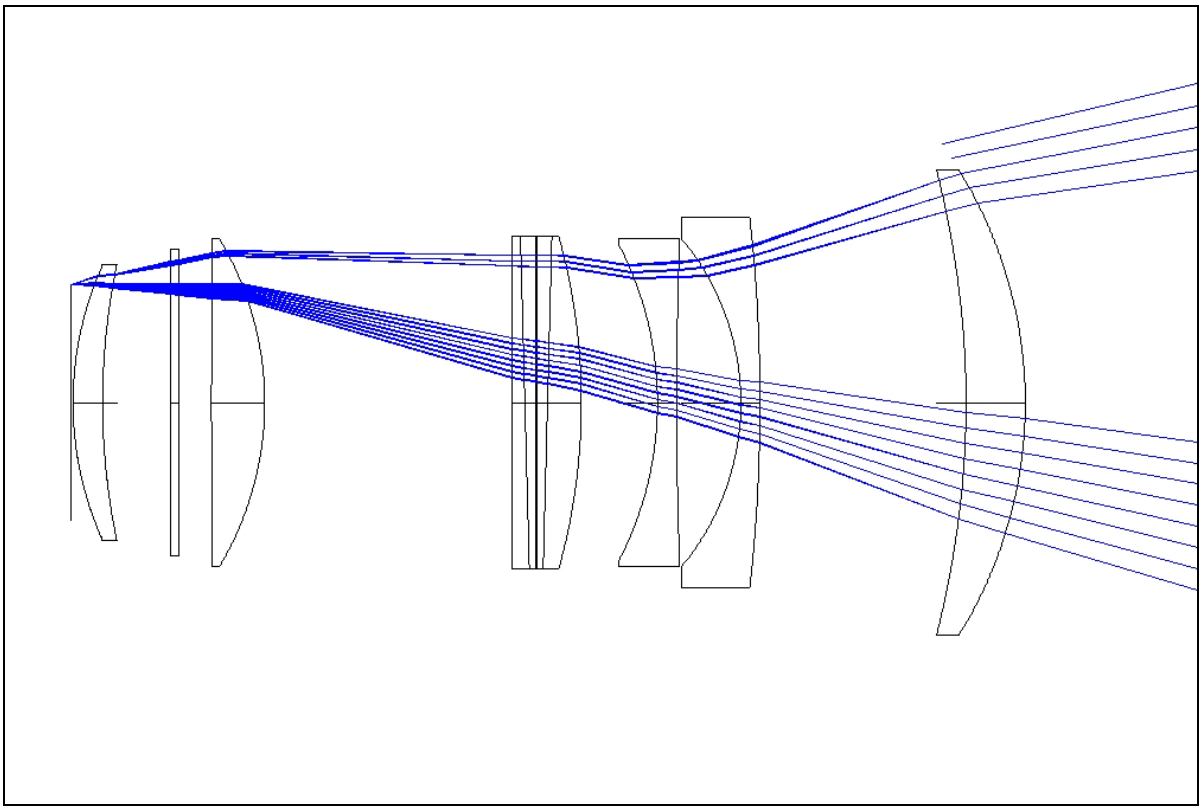

Figure 1: Optical layout of 3.0-deg prime focus corrector for the Discovery Channel Telescope

If operation of two telescopes with 4.2m apertures is not of interest, then the prime focus corrector for the DCT can be redesigned to image a 3.0 deg area of sky. Some believe this to be an exceedingly difficult task, but here we present the optical layout for such a corrector, complete with a built in atmospheric dispersion corrector (ADC), something lacking in the DSST design. The ADC is important for correcting the chromatic smearing of the atmosphere at large angles away from the zenith. The optical layout of the larger DCT corrector is shown in figure 1 and its performance is provided in figure 2.

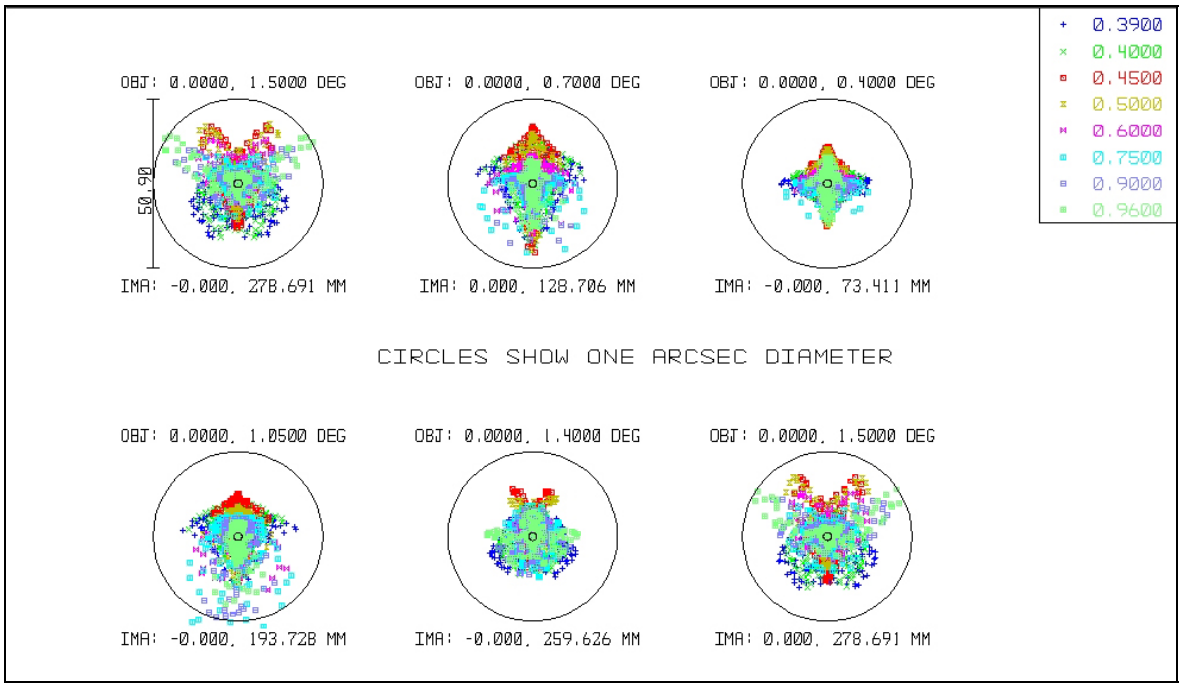

Figure 2: Optical performance of 3.0 deg PFC for Discovery Channel Telescope. Ray-traced analysis indicates spots less than 1-arcsec diameter

The DCT with 3.0 deg PFC results in a final etendue of 55.2m^{2}deg^2. This is very impressive for a single telescope and greatly exceeding the performance of the DSST. Cost of the DCT system with enlarged field PFC is estimated to be $40M with most of the additional cost going into the larger focal plane array. Optical costs should be within $1M of the 2.0 deg design.

Better optical designs represent only half the problem. The other problem which needs to be addressed is that of search strategy and detection algorithms. Figure 3 shows the anticipated detection thresholds for a 600-mm aperture telescope with a focal ratio of f/1.25. Here we are not concerned with the absolute search rate, but rather the detection strategy. The figure shows anticipated detection threshold using typical detector values, for space objects moving at the angular rates indicated.

This figure clearly shows that as target angular velocity increases and integration time increases, detection thresholds actually deteriorate. This is because the target spot has moved off the first pixel it was on since the shutter was opened. As exposure time increases the target contributes no more signal to the pixel in question, but sky brightness and noise sources continue to negatively impact the pixel.

This figure is important for two reasons. The first is related to detection of satellites at high altitudes. A satellite in geostationary orbit moves across the star field at a rate of 15 arcsec/sec. For a telescope fixed to the earth, staring at the celestial equator, the geostationary satellite appears to stand still on the focal plane and continues to integrate on a single spot. Hence, even a small telescope can achieve significant detection thresholds with modest integration times. For all objects not in a geostationary orbit however, detection thresholds are reduced. For example, a

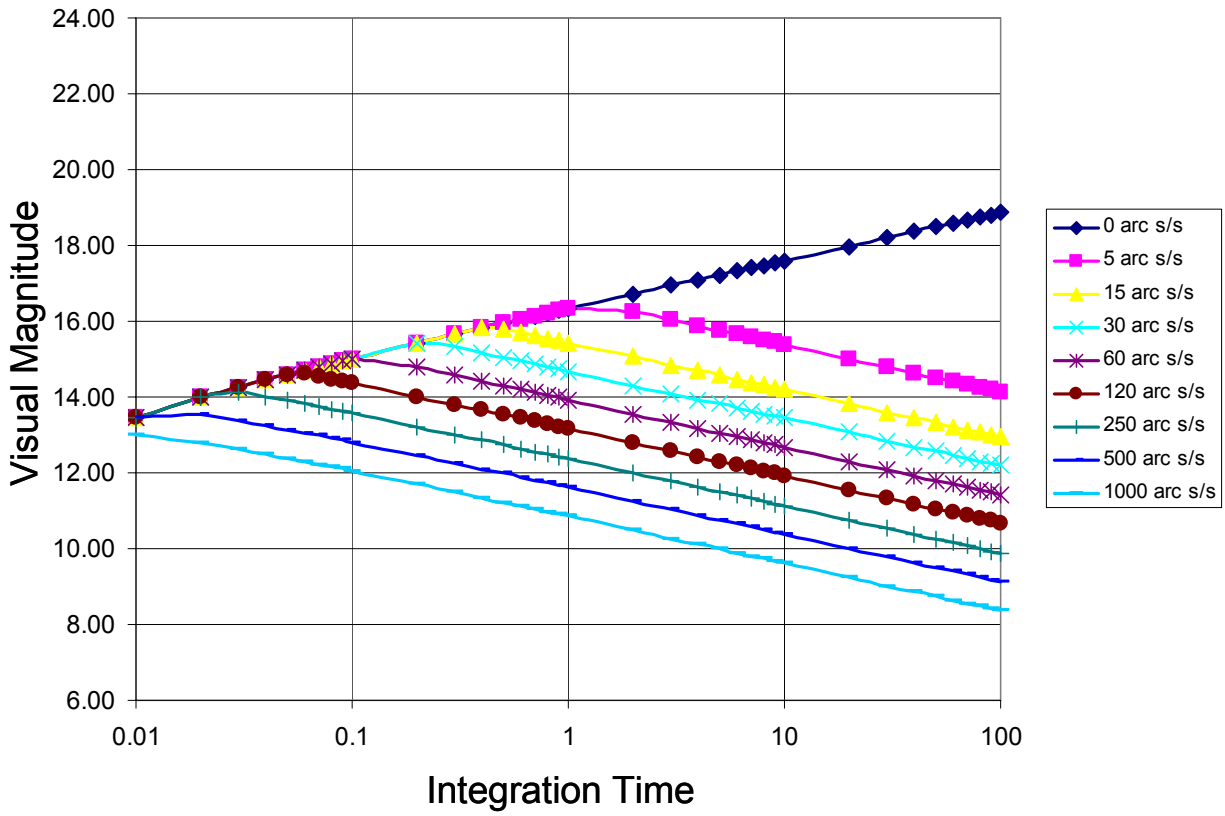

Figure 3: Detection threshold for 600mm telescope as function of target angular rate. Integration time is shown on the x-axis while visual magnitude is shown on the y-axis

satellite at the geostationary altitude, but inclined 90deg would again experience a translation rate of 15arcsec/sec. For any satellite in an inclined orbit, detection thresholds are reduced.

The second significant feature of the above figure is what is now shown. The figure shows the impact on satellites with angular rates of up to 1000 arcsec/sec. Low altitude satellites can experience real angular rates of several hundred arcsec/sec, but effective angular rates of several thousand arcsec/sec. Low-earth-orbit satellites are therefore extremely difficult to detect with a staring system unless they are very bright.

As for search strategy, when looking for LEO objects, where do you look? The sky is a very big place, and even very wide-field telescopes only examine a small portion of the sky in any single image. It is believed here that staring systems offer the best overall performance given that one has no idea from which direction a piece of space debris will appear, or what direction it will be going. Only a staring system can capture all directions of motion equally. Staring systems, however, have the limitation of detection threshold as seen above. What is needed is a new approach to extracting target information from images made with staring telescopes.

As part of this study, we examined the claims of an independent external consultant and approached his claims as a chance to do some technical "Myth Busting." Details of the technical approach are not presented here to protect proprietary information, but the new approach to image processing and noise reduction was explored for a single altitude target (due to the complexity of the algorithms and the limited time to adapt them to other orbits). The claim was

that with proper signal processing, streak detection and noise reduction, it would be possible to gain two magnitudes of detection performance against traditional streak extraction approaches for staring telescopes. An improvement of two visual magnitudes represents an increase in sensitivity of a factor of roughly 6.25, or a decrease in required telescope aperture on the order of a factor of 2.5.

We were able to theoretically verify the claims presented to us. For a 600-mm aperture telescope with an f/1.25 focal ratio, we were able to show that for a target at 600-km altitude, moving at a real rate of approximately 225 arcsec/sec, detection thresholds for the modified algorithm improved detection threshold from visual magnitude 9.84 to 12.83, an increase of two visual magnitudes. Improvements at other altitudes were briefly explored, but due to the complexity of the signal processing, few additional results are available. Improvement in sensitivity at higher altitudes was noticeable, but not of the same order of magnitude as at lower altitudes.

Sample Russian Space Object Imaging Development Programs

The Russian Space Agency, with the participation of Russian Academy of Sciences institutes, is developing various space-object-imaging capabilities. Given that space debris removal is a common international concern, Russian and Sandia scientists have engaged in discussions regarding potential collaborative efforts to develop and field a space-debris removal system. The scope of these discussions and initial studies has included space debris detection, tracking, ranging, targeting, imaging, and laser neutralization concepts. However, given the pivotal importance of space object identification (i.e., discriminating space debris versus micro-satellites), this report focuses on the imaging aspects of these collaborations. Specifically, included in the following sections are a description of the Sapsan imaging system concept, space-object illumination concepts, and potential space imaging approaches that mitigate atmospheric turbulence degradation effects.

Meetings were conducted at the Altai Laser Optical site in Russia in June-July 2008 with the intent of touring the site, participating in ground-to-space laser ranging and space-object imaging demonstrations, and to discuss options for developing a space-object imaging capability for potential application in space-debris detection, identification, and removal. This site, which is adjacent to the village of Savvushka in the Zmeinogorsk region of the Altai territory of Russia, provides precision ranging and angular measurements of spacecraft. Key Russian participants in this meeting included Professor Victor Daniilovich Shargorodskiy (First Deputy to the General Director at the Russian Space Agency's Science Research Institute for Precision Instrument Engineering (FSUE-IPIE), Moscow; niipp@niipp-moskva.ru), Evgeniy Grishin (FSUE-IPIE; e-grishin@niipp-moskva.ru), Sergey Novikov (IPIE, Director of the Altai Site; sbn1308@rambler.ru), Evgeniy Shulov (FSUE-IPIE; shulov@niipp-moskva.ru), Dr. Alexander Mikhailovich Sergeev (director of the non-linear optics division and deputy director of the Russian Academy of Sciences Institute of Applied Physics (IAP) in Nizhny Novgorod; ams@utp.appl.sci-nnov.ru), Dr. Oleg Valentinovich Kulagin (a senior scientist of the Institute of Applied Physics in Nizhny Novgorod, Russia, expert in phase conjugation, nonlinear optics, and laser physics;mok@appl.sci-nnov.ru), and Pavel Inshin (ASC Femto, Moscow; expert in adaptive optics; inshin@femto.ru).

Figure 4: Photograph of the main meeting participants pictures at the entrance to the ranging and imaging telescope radome at the Altai Laser Optical site

SAPSAN Imaging Concept

During discussions at the meeting, the Russian team proposed the development of a new optical ground station that would be designed for:

- Autonomous detection as well as detection using ephemeris of low-orbit space objects;
- Determination of angular coordinates and photometric characteristics of space objects;
- Obtaining low-orbit space object images with near-diffraction-limited imaging under sunlight illumination conditions using an adaptive optics system;
- Obtaining low-orbit space object images with near-diffraction-limited imaging using concentrated laser illumination of the space object. The concentrated laser would provide higher illumination beam quality for improved day-night imaging.

To provide for autonomous detection, the system would need a wide field of view (i.e., hundreds of square degrees) telescope that would continuously reorient the field of view along the trajectory of the moving space object in a piecewise staring mode with overlapping incremental fields of view. Beyond detection, non-imaging photometrics data is needed to characterize the imaged space object. Unlike an active spacecraft, space debris is not stabilized in space and it rotates randomly under the influence of various forces (e.g., solar pressure, atmospheric drag,

Table 1: Integral brightness of space object in the visible band (star magnitudes).

Distance, km	Space object size, cm				Angular velocity, arc degrees/sec
	5	10	20	40	
200	9.8	8.3	6.8	5.3	1.9
400	11.3	9.8	8.3	6.8	1.0
800	12.8	11.3	9.8	8.3	0.5
1,600	14.3	12.8	11.3	9.8	0.12
5,500	17.0	15.5	14.0	12.5	0.07
20,000	19.8	18.3	16.8	15.3	0.012
36,000	21.1	19.6	18.1	16.6	~0.001

etc.) that cause rapid changes in the reflected sunlight flux. Measuring the time spectrum of change in the light flux reflected from space debris and solving the inverse problem to determine the object parameters, one can obtain estimates of the geometric characteristics of space debris even when angular dimensions of the observed debris are significantly smaller than actual resolution of the telescope. Though the photometric signal measured from the rapidly changing 3-D orientation can typically help distinguish between debris and microsatellite, according to Professor Shargorodskiy, Russian satellites are sometimes intentionally reoriented quickly or are designed to rotate in a manner that would provide a similar spectrum signature. As a result, detailed imagery is needed to reliably identify and characterize space objects.

This proposed imaging system, called Sapsan (Russian for Peregrine Falcon), would be composed of the following three functional modules:

- An optical-system module for autonomous detection, angular coordinates measurement, detailed imaging and concentrated illumination of the space object;
- A module for system control and space object information collection to support cataloging and data storage;
- A support module that contains the full system infrastructure (e.g., timing, electronics, etc.) to make the system elements an integrated operational capability.

One challenge encountered by any proposed space object imaging system is the need for sufficient lighting to produce an image. In the reflected sunlight, space object brightness drops proportionally as a function of (1/distance^2). The brightness of sun-illuminated space objects can be expressed in terms of star magnitudes using:

$$M_v = 5.0 \log L - 5.0 \log d - 2.5 \log \left[1/\pi \sin\theta + \cos\theta \left(\pi - \theta/\pi \right) \right] + C \ , \qquad (1)$$

where

L – distance to the space object, km,
d – space object diameter, cm,
θ – phase angle,
C – constant depending on space object shape and its albedo.

The 3rd term of equation (1) $\{(\sin\theta)/\pi+(\cos\theta)(\pi-\theta)/\pi\}$ is called the phase integral of the Lambert surface of a sphere. The uncertainty in the albedo and phase integral of the space object is the only reason for uncertainty in the calculation of its star magnitude. As a rule, the well-known phase function of the Moon, shown in reference [2], is used to mitigate this uncertainty. The star magnitude of space objects at any phase may be defined through the star magnitude of the Moon at zero phase M=-12.73. Setting the Moon albedo at 0.1 and using the angular diameter of the Moon (0.5°), we can compute the constant in formula (1) as C=1.8. Calculations of the integral brightness of space objects using formula (1) for the albedo of 0.1 and $\theta = 0^o$ versus typical values of the parameters and range are presented in Table 1. The last column of the table contains typical angular velocities for space objects at the given orbital altitude.

The last two lines of table 1 show brightness for the high-orbit space objects. On average, low-orbit space object brightness is two orders of magnitude (5 star magnitudes) brighter than high-orbit one and the angular velocity of the low-orbit space objects is an order of magnitude higher than the high-orbit ones.

Figure 5 shows the atmospheric absorption versus zenith angle, expressed in star magnitudes. Figure 5 shows that detection of extremely weak reflected light signals from space objects at zenith angles greater than 75° is not feasible due to large losses due to atmosphere absorption, particularly as the atmosphere transparency decreases. This is one reason why telescopes are frequently located in high-mountain locations where the atmospheric transparency is higher (and local light pollution is less).

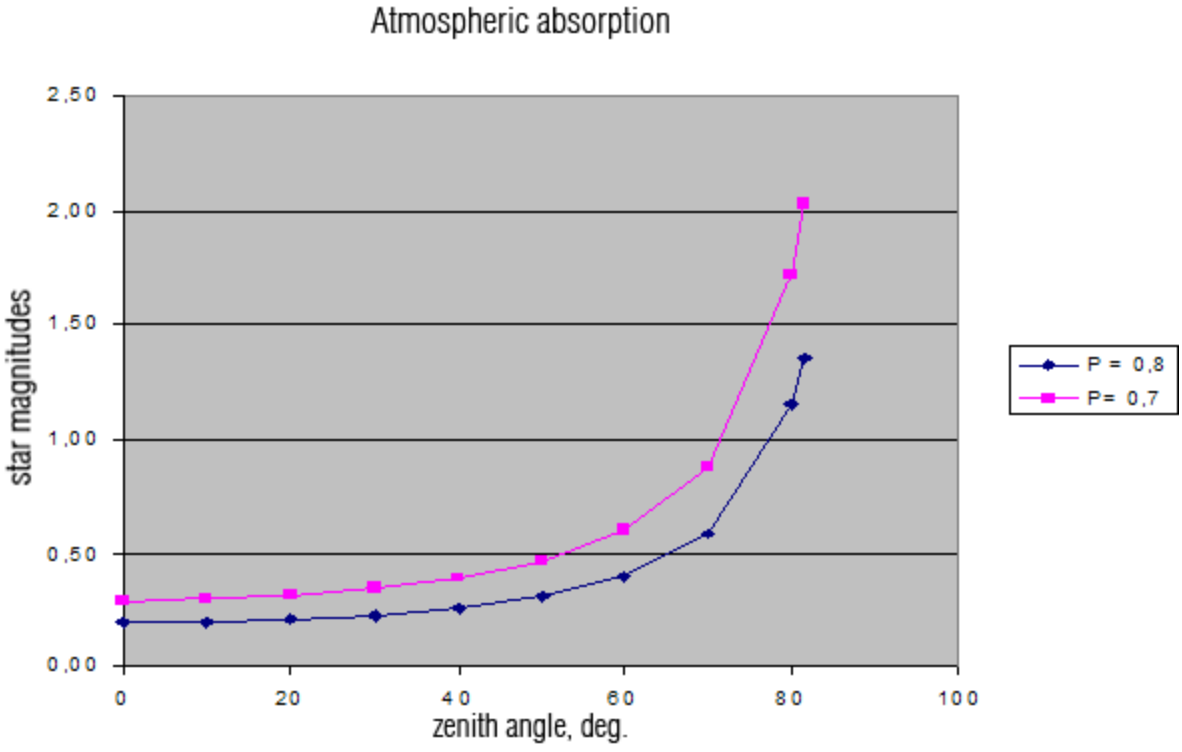

Figure 5: Atmospheric absorption losses (star magnitudes) encountered during space object imaging at different zenith distances for two cases: a) p = 0.8 – normal transparency of atmosphere; b) p=0.7 – visible haze in atmosphere

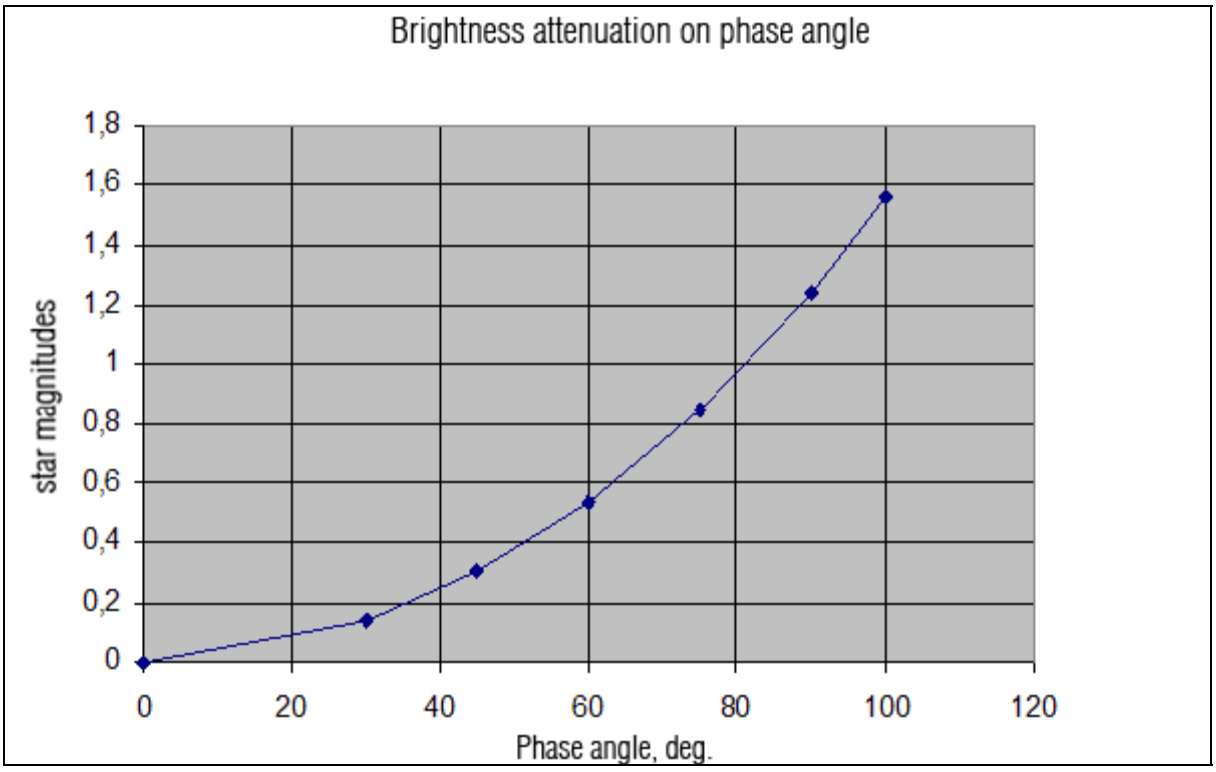

Figure 6: Attenuation of space object integral brightness as a function of the phase angle in terms of star magnitudes

The dependence of the space object brightness attenuation on phase angle is shown in figure 6. Observations of space objects at phase angles greater than 80° experience attenuations of the space object brightness of more than one star magnitude and therefore are not feasible.

To address these dim space-object imaging challenges, the Sapsan system concept proposes the use of a laser illumination system to overcome the imaging challenges created by the signal attenuation and reliance on sunlight illumination. The details of the illumination system and its nonlinear optical approach for concentrating the laser and mitigating turbulence effects are discussed in later in this repor.

SAPSAN Imaging System Design

The Sapsan system consists of two telescopes. The first is a detection system used to locate space objects. The second system, referred to as the informational channel, is used to characterize a detected space object. The informational system operation would be fully automated. The main characteristics of the system module for autonomous detection, angular coordinate measurements, detailed imaging, and concentrated illumination of the space object are as follows:

Table 2: SAPSAN imaging system characteristics

Characteristics	Value
Working field of view of the system with 2 telescopes of Ø200 mm «Sapsan-200» (square degrees). Used to search for objects.	144
Working field of view of the system with 2 telescopes of Ø125 mm «Sapsan-125» (square degrees).	800
Surveillance rate of the system with two telescopes «Sapsan-200» (sq. degree/hour) with 4 exposures at each point.	87,600
Sensitivity of the system with two medium telescopes «Sapsan-200» (with the night sky brightness of 21^m per one square second of the celestial sphere) for space objects at 1500 km (corresponding to minimum space object size of 1.5 cm when using ephemeris and 8.2 cm in random detection mode).	13.1^m
Sensitivity of the system with two telescopes «Sapsan-125» for space objects at 400 km (corresponding to minimal space object size of 1 cm when using ephemeris data and 14 cm in random object detection mode).	9.1^m
RMS measurement error of the space object angular coordinates using the «Sapsan-200» two telescope systems.	$\leq 1.2''$
RMS error of measurement of the space object angular coordinates using the «Sapsan-125» two telescope systems.	$\leq 5''$
Working field of view of the system with informational lens Ø1000-1500 mm «Sapsan-1000» (arc seconds). This is the region with the best sensitivity – the full system field of view is larger.	40-60
Number of control zones in the flex mirror of the adaptive optics system (AOS) (ea.). The flex mirror is a deformable mirror device.	90-120
Type of laser used for illumination (pulsed)	Fiber-optics, single mode, with diode pumping
Power of the illumination laser (KW)	3-10
Laser wavelength (μm)	1.03-1.07
Achievable angular resolution in the space object detailed imaging mode and minimum size of the spot focused on space object surface (arc seconds)	0.1-0.2

To achieve an angular resolution of 0.1 arc seconds at the specified wavelength would require a telescope diameter on the order of 2.6 m. Reducing the telescope diameter would increase the minimum achievable angular resolution.

The proposed system would use a two telescope configuration. The field of view of the system with two lenses (Ø200 mm) is 2 × 8.50 degrees × 8.50 degrees, which is sufficient for imaging detected objects but which is not adequate for detection of the fast-moving "falling" space objects. The angular speed of such low-orbit space objects is greater than 3 degrees/sec. Therefore, we propose to use a second system with two smaller lenses (Ø125 mm) to provide a field of view of 2 × 20 degrees × 20 degrees. The combined field of view of this dual configuration system would be 800 sq. degrees, thereby increasing the probability of obtaining

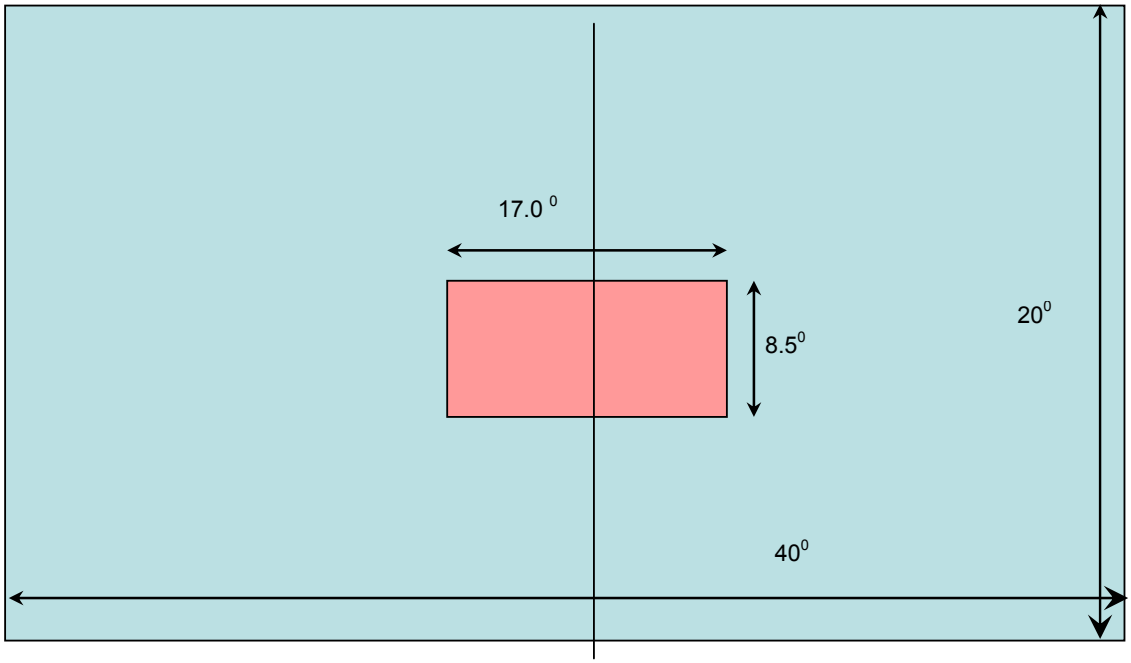

Figure 7: Mutual position of fields of view of 2 «Sapsan-200» and 2 «Sapsan-125» lenses. The system with the larger field of view would have a sensitivity of 9m and the sensitivity of the system with the smaller field of view is 13m

the necessary number of measurements for the lowest orbit space objects. This dual field of view configuration is illustrated in figure 3.

Figure 8 provides a functional layout of the proposed optical system for concentrating the laser illumination on the space object and for acquiring detailed images of small objects under either sunlight or concentrated laser illumination. The blue lines in figure 4 define the path of the sunlight reflected from the object to the primary mirror, then to the adaptive secondary mirror that is used to compensate for the atmospheric distortions and system jitter, and to make some phase corrections. The secondary mirror can be moved in multiple directions.

The image is sent from the detector to a personal computer (PC) to be used to control the laser mirror. The deformable secondary flex mirror (deformed based on sunlight return) performs the pre-compensation of the outgoing laser. The laser is pulsed such that the beam is off when the signal returns from the illuminated space object. The deformable secondary mirror (DMD) follows the reflected sunlight signal and updates its shape accordingly. As designed, the laser return from the target is shifted so it will not pass through the mirror aperture to the visible band detector. The spectral divider and the mirror below the DMD are dichroic mirrors. The flex mirror control module is a phase front detector.

The laser beamwidth control mirror will likely have a dielectric coating and it will have a limited number of adaptive optics modes so that in addition to pointing it can also perform some adaptive focusing (mirror curvature) for use when illuminating and imaging larger space objects (> 1 arcsec) or for focusing on specific areas of interest on a space object.

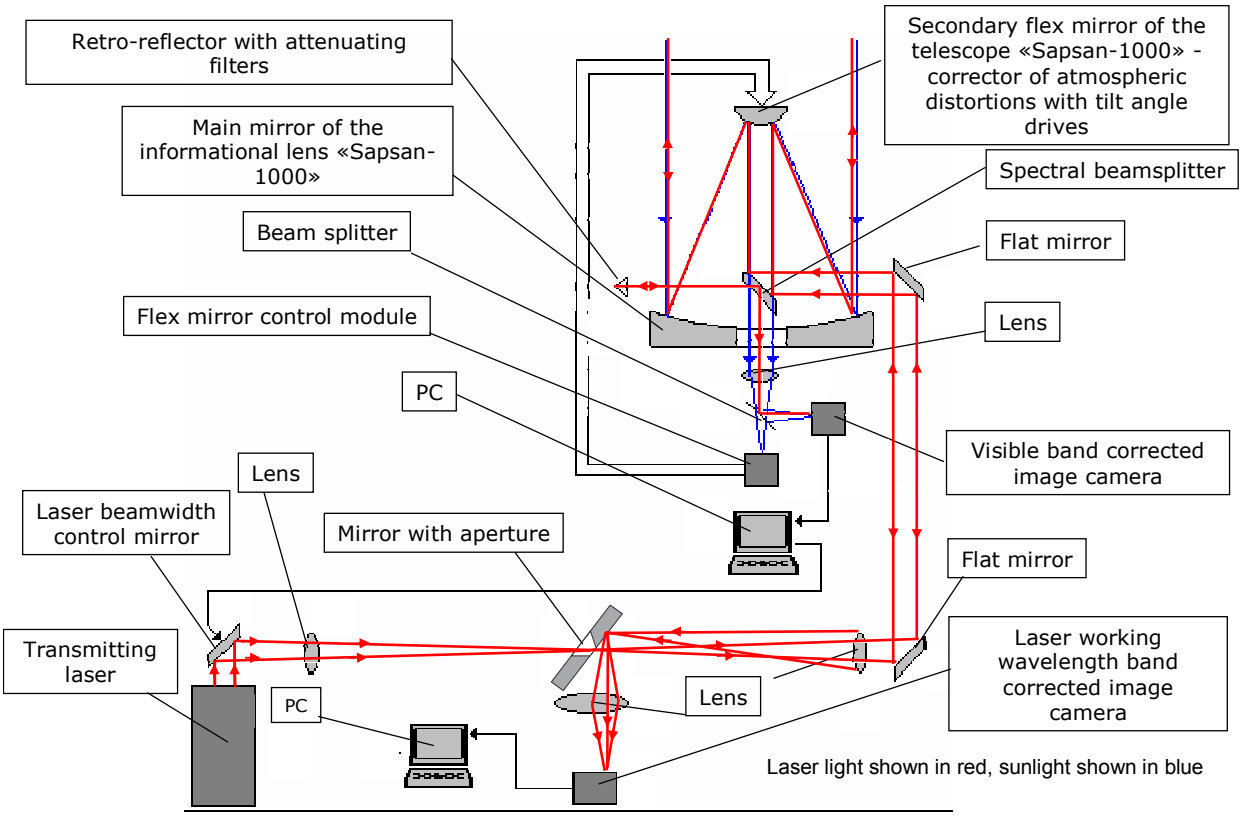

Figure 8: System diagram illustrating the illumination concentration channel and the detailed imaging channel using either sunlight or laser illumination

Figure 9 provides a more detailed design layout for the secondary mirror used to correct for atmospheric distortions. This mirror will be actively cooled.

The secondary control mirror can be translated in three planes using piezo actuators. The reflecting concave membrane is connected to 100 piezo actuators that can be moved 2-3 microns. These actuators should provide the capability to control the mirror with accuracy better than one-tenth of a wavelength with a response time in the feedback loop of no worse than 1 msec. The brace shown in view **A** supports the secondary mirror. The three steel cups are piezo actuators positioned in a triangular orientation with no center of mass motion.

The isoplanatic angle limited by the atmospheric turbulence differs based on various factors including the telescope location. For example, at the Altai site they typically experience about 5 arc seconds of isoplanatism in the visible region and about 10 arc seconds at a wavelength of 1 micron. Alternately, at the Russian Miadanak Measurement Center (on top of 2750 m high mountain) the isoplanatic angle is much better with typical values ranging from 20-30 arc seconds.

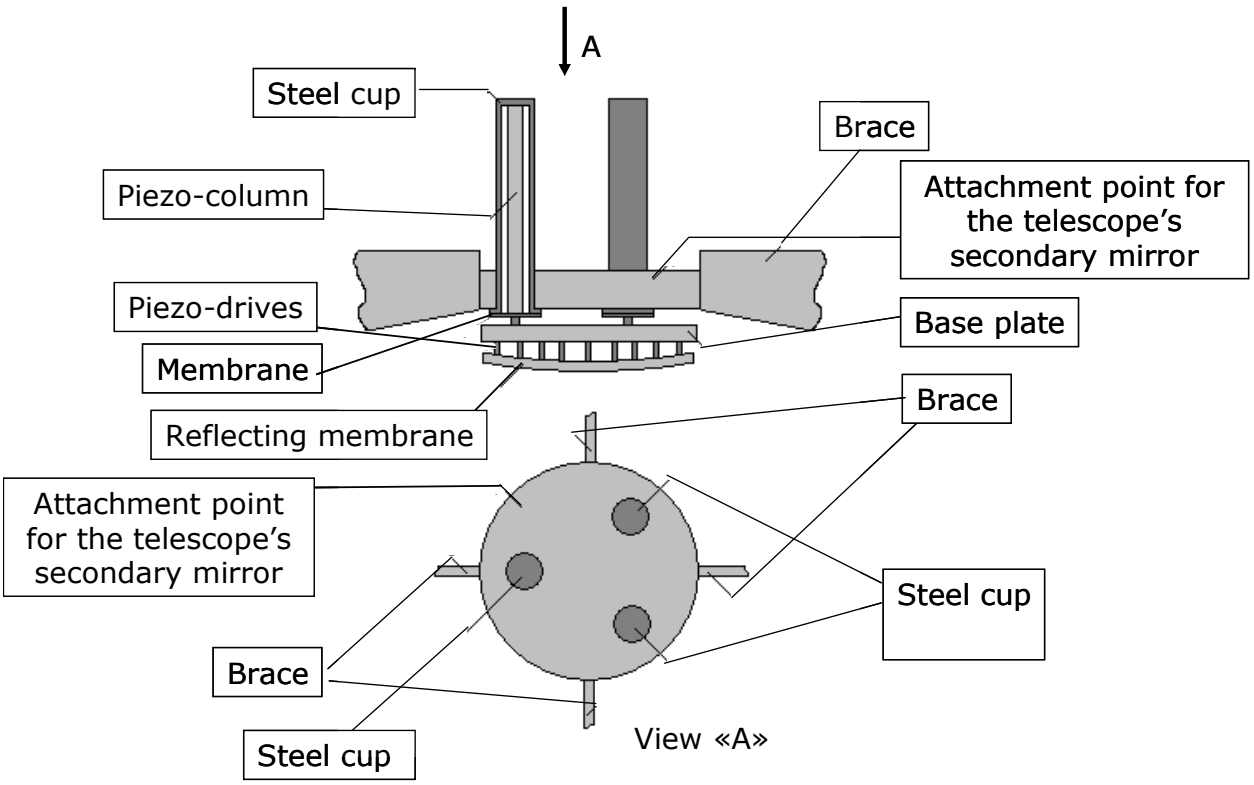

Figure 9: Diagram of the secondary flex mirror for the informational lens system «SAPSAN-1000»

The intent of the system control and information collection module is:

- Daily and operational planning of sessions to search and observe space objects;
- Implementation of the automatic cycle for search, detection, tracking of space objects, formation of coordinate and non-coordinate measurements of space objects;
- Logging and display of the results from functional checks of system hardware and software;
- Maintaining the frequency catalog of the space object coordinate and non-coordinate characteristics;
- Archiving the obtained measurement information and the processed results.

The intent of the support module is to provide

- Provisions for the necessary set of synch frequencies and time tags to the system (e.g., quartz standard system, coordination with Glonass);
- Provisions for the necessary system meteorological data (pressure, humidity, temperature;
- Provisions for interaction between system's hardware components by means of fiber-optics communication system;
- Telescope shelter – a tower with 2-leaf dome, foundation, power supply, data transfer, utilities on site.

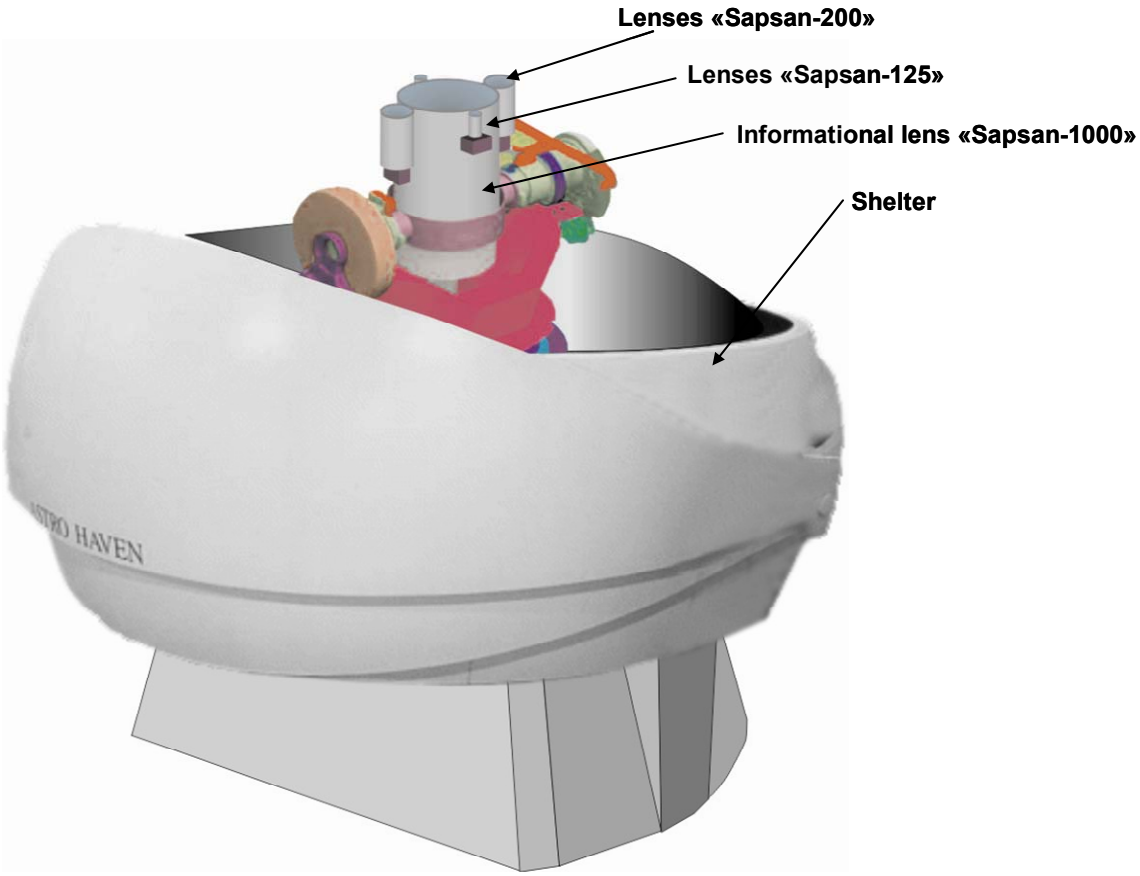

Figure 10: Sapsan system rendering

Figure 10 provides a rendering of the integrated telescope modules in a single mount with an enclosure. The lenses are the telescopes used to detect and characterize (informational lens) space objects.

As identified above, adaptive optical elements are integrated into the Sapsan system. However, additional concepts are under consideration. In terms of adaptive capabilities, Pavel Inshin (ASC Femto, Moscow**)** is working on the development of a more advanced adaptive optics system that would be used with a 3.12 m telescope. This future system would contain three adaptive optical (AO) systems that contain a total of 400 actuators. This system would treat the atmosphere as if it were three independent phase screens and then attempt to control the AO systems to correct for each of these three layers. These AO systems will be operated using controlled laser illumination and focusing to engineer glints which would act as point sources for the AO control system as opposed to strictly relying on sunlight illumination and natural glints.

Application of highly sensitive nonlinear optical methods for imaging space debris

Insufficient space-object light levels and atmospheric turbulence effects preclude high quality day-night imaging. As part of the Saspsan concept to detect and image small space objects, it is proposed to use a low-energy laser illumination source and a highly sensitive receiver to collect and amplify the light scattered from the object, combined with a phase conjugation approach for minimizing the laser energy requirements and for mitigating atmospheric turbulence. This approach builds on the foundation research performed by Kulagin, Pasmanik and Shilov.[11]

The proposed optical-brightness amplifier consists of a traditional Nd:Glass laser amplifier and a nonlinear optical amplifier. By amplifying the space-object-reflected illumination (a factor of $10^{12} - 10^{14}$ is achievable) it is possible to eliminate the challenges of imaging low light space debris. By virtue of a narrow frequency reception band ($\sim 10^{-3}$ cm^{-1} = 30 MHz) and the short turn-on time ($\sim 0.33x \cdot 10^{-8}$ s), we believe the Sapsan optical brightness amplifier concept should allow us to detect and image space objects at any time of day, including under bright sunlight conditions, presuming a view to the space debris is not completely occluded by clouds. The problem may be formulated as follows. Laser radiation illuminates space within a given angle. Part of this radiation is diffusively scattered by the hypervelocity space object and is intercepted by a telescope receiving system and then registered on a CCD camera. In the receiving system, light collected by the telescope is pre-amplified in the optical brightness amplifiers. After the amplifiers, the level of useful signal should be sufficient to be recorded by ordinary means.

One of the key advantages of the optical brightness amplifiers is that they have nearly 100% quantum efficiency. In fact, the noise floor is about 2.5 photons, so the amplifier can begin to respond to signals as low as 3 photons. Further, because of their narrow reception band ($\Delta\lambda \sim$ 0.001Å) and short reception time (~30 nanoseconds), background noise from the daytime sky will be insignificant during daytime operation of the system with optical amplifiers. Though the amplifier can respond to as few as 3 photons, we consider the signal detected if the signal-to-noise ratio is above six, which corresponds to our criterion for reliable signal detection. Further, for providing sufficient resolution to image the contours of the space object, we believe the number of images pixels should be no smaller than 100 (i.e., 10 × 10 image pixels). Hence, when considering images acquired with conventional imaging telescopes as opposed to our proposed system with optical amplifiers, we believe that our system can provide higher resolution. And, in addition, the narrow reception band and small turn-on time of the system with optical amplifiers should be capable imaging any time of day, unlike a conventional charge-coupled system. Also, the optical-brightness amplifiers allow for the use of a much smaller telescope aperture for the same amount of laser illumination energy. For example, calculations show that for a 60-cm-diameter telescope, seven times less laser energy is required for a system with optical amplification than for a system using a conventional cryogenically cooled low-noise CCD. Even less energy is needed when phase conjugation approaches, such as those discussed below, are employed.

The concentration of the space-object-reflected laser illumination is restricted by the influence of turbulence. However, to keep the required laser energy sufficiently low for practical applications, we must develop a way to quickly compensate for the dynamic turbulence effects. If the illumination energy is fixed, the illumination pointing must be narrowed. Such illumination

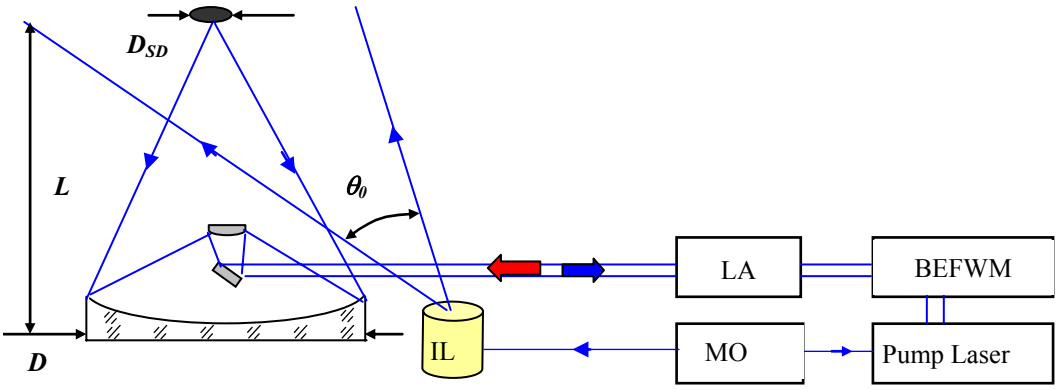

Figure 11: System schematic. IL – illumination laser; LA – laser amplifier; MO – master oscillator; BEFWM – Brillouin Enhanced Four-Wave-Mixing system

concentrating can be achieved by means of phase conjugation of scattered illumination using nonlinear optical methods. If our nonlinear-optical receiver amplifies and conjugates the space object signal, then as a result of double passage through the atmosphere turbulent distortions of the reflected signal will be significantly compensated. As a result, the conjugated signal will be concentrated on the space object to an accuracy that is determined not by the turbulent scattering angle ($\sim 10^{-5}$ rad), but by the receiving aperture of the nonlinear optical amplifier (e.g., $\sim 5 \cdot 10^{-7}$ rad for a 200-cm receiving aperture).

Space Object Illumination Operating Concept

The space-object-reflected illumination light is intercepted by the main mirror of a receiving telescope (such as the Sapsan telescope) and is guided to the optical brightness amplifiers. Upon amplification in the optical amplifiers, the light is registered with a CCD camera. A control system is used to turn on the optical brightness amplifiers and adjust their reception frequency band. Data for the control system are provided by an illumination laser (IL) and a rangefinder (estimates moment of arrival of the scattered radiation and its frequency). The optical brightness amplifiers consist of three units: a laser amplifier (LA), a nonlinear optical amplifier and a pump laser. To achieve the lowest level of noise in the optical brightness amplifiers, the gain coefficient in laser amplifiers must be about 10^4. Such a gain coefficient can be achieved in two amplification stages. When creating the laser amplifiers, it is necessary to ensure that the value of the gain coefficient is uniform over the whole field of view. The latter, in turn, should be not less than the angle of initial illumination $\theta_0=10^{-4}$ which requires the use of optical repeaters. The space object plane is projected by a lens onto the output face of the first laser amplifier. The image is then transferred by a repeater from the output face of the first laser amplifier to the input of the second laser amplifier. Another repeater transfers images from the output face of the second laser amplifier to the nonlinear optical amplifier. The repeater is a confocal telescope.

The nonlinear optical amplifier is a Brillouin-enhanced four-wave mixing (BEFWM) amplifier (i.e., a third order nonlinear medium that is active with respect to the Brillouin nonlinearity). For such a medium to amplify signal light, it should be illuminated simultaneously with the space-object-reflected signal and by a powerful additional laser radiation pump. Typical nonlinear

medium elements are tetrachlorides such as CCl_4, $GeCl_4$, $SnCl_4$, or perfluorooctane. Their parameters are very similar (e.g., nonlinearity factor ~ $5x10^{-9}$ cm/W, hypersound relaxation time ~10^{-9} sec). When the stimulated-Brillouin-scattering (SBS) cell is illuminated by a pulsed laser with a pump of energy 1.5 J and duration of 20 nanoseconds, the SBS amplifier will amplify the space-object-scattered light with a gain coefficient of approximately 10^8. Therefore, the gain coefficient of light received from the space object, consisting of combined gain in laser amplifier and nonlinear optical amplifier, will be about 10^{12}, which is quite adequate to record the signal on a CCD.

Application of phase conjugation methods for concentrating the illumination of space debris

The concentration of the space-object-reflected laser illumination is restricted by the influence of turbulence. To improve imaging and to reduce the required level of illumination laser irradiance requires that we overcome the atmospheric turbulence to focus the beam. We believe this can be achieved through optical phase conjugation of illumination radiation using nonlinear optical methods. Optical phase conjugation (OPC) methods use nonlinear optical techniques to reverse the beam propagation direction and phase to compensate for the atmospheric distortions as the beam back propagates through the optically distorting path. If our nonlinear-optical receiver amplifies and conjugates the signal intercepted by the receiving lens, then as a result of double passage through the atmosphere, turbulent distortions of the space-object signal wavefront will be significantly compensated. Consequently, the conjugated signal will be concentrated on the space object to an accuracy that is determined not by the turbulent scattering angle (~10^{-5} rad) but, instead by the resolution of the receiving aperture of the nonlinear optical amplifier (e.g., ~ 5 × 10^{-7} rad for a receiving aperture of 200 cm).

Possible alternatives for performing optical phase conjugation include stimulated scattering (e.g., Stimulated Mandelstrom-Brillouin Scattering, Stimulated Kerr Scattering, Stimulated Raman Scattering, Stimulated Rayleigh Scattering, etc.) and four-wave-mixing (FWM) schemes in resonantly absorbing and photorefractive media. These approaches have been investigated for various applications in the past and the concept of optical phase conjugation for concentrating illumination together with input signal conjugation to amplify the signal has been demonstrated in lab environments, but not in long range outdoor arenas [10]. Of the various techniques, we believe the optical-phase-conjugation method using four-wave mixing of light and hypersound (Brillouin Enhanced FWM - BEFWM) is the most viable for space object imaging. BEFWM is the most attractive for potential space object imaging applications because of its simplicity, efficiency/high sensitivity, relatively wide angle of vision, sufficiently wide dynamic range, and inherently short response time. Further, when the four-wave mixing occurs in the regime of absolute instability, phase conjugation is possible with high reflection coefficients (R~ 10^6 - 10^7) limited only by the effects of pump wave saturation. In this case BEFWM is essentially a nonlinear optical amplifier with high gain coefficient (amplification with a total gain of 10^{15} has been achieved [12]). Finally, BEFWM has the highest operating speed (~ nanosecond) when compared to the alternative methods (1 msec – 1 sec), which is critical for space object illumination and imaging.

To consider the viability of the proposed technique, we performed some very preliminary calculations specifically including losses during transmission/reception, reflection from the moving space object, propagation through atmosphere (including turbulence) and depolarization

of the illumination light. As shown in table 3, we estimate that a pulsed laser with illumination energy of 10 J can be used to observe a 20 cm space object using the BEFWM optical receiver if the distance to the space debris is not much more than 100 km. We also estimate that this distance for space object observation will increase if the laser illumination is concentrated using the proposed optical-phase-conjugation approach. As shown in table 4, by using one concentration feedback step we should be able to extend the operating range from 100 km to more than 400 km for the same 10 J level of laser illumination. Further, by adding a second concentration step we can further extend the operating range to almost 700 km without increasing the laser power. In principle, it should be possible to further increase the number of concentration steps to extend the range for the given laser power level, but every such step complicates the BEFWM pump scheme and pre-amplification scheme. Also, we are concerned that any further increase of the maximum observation distance might require a decrease in the angle of initial illumination, which corresponds to the angle of vision. This would create other challenges to overcome, so we believe the practical solution to extend operating ranges beyond 700 km will likely involve increasing the laser pulse energy beyond 10 J, which is easily done. Nevertheless, theoretically this proposed nonlinear optical approach offers the hope of observing small high-speed space objects at any time of the day. However, this theory must be validated in relevant testing.

Table 3: Minimal illumination energy for space debris observation by BEFWM image amplifier without concentration

L_0, km	100	200	300	400	500	600	700	800	900	1000
W_0^{min}, J D_{SD}=0.1m	15	240	1200	3800	9300	$1.9\cdot10^4$	$3.6\cdot10^4$	$6.1\cdot10^4$	$9.7\cdot10^4$	$1.5\cdot10^5$
W_0^{min}, J D_{SD} =1 m	0.15	2.4	12	38	93	190	360	610	970	1500

Table 4: Minimum space-debris-illumination energy at one-step and two-step concentration.

L_0, km	300	400	500	600	700	800	900	1000
K_{eff}	52.1	29.3	18.8	13.0	9.57	7.33	5.79	4.69
W_0^{min}, J; 1 step	1.85	10.5	39.5	120	295	660	$1.35\cdot10^3$	$2.5\cdot10^3$
W_0^{min}, J; 2 steps D_{SD} = 0.1m	$3.6\cdot10^{-2}$	0.36	2.1	9.0	31	90	235	540
W_0^{min}, J; 1 step	0.26	1.0	3.8	12	29	64	130	243
W_0^{min}, J; 2 steps D_{SD} = 1 m	$4.9\cdot10^{-3}$	0.034	0.2	0.88	3.0	8.7	22	52

Technical Challenges

When radiation reflects from a moving space object, it creates a frequency shift (Doppler effect) in the reflected illuminating laser pulse. For the reflected pulse to be within the reception frequency band of the proposed optical amplifiers, two conditions must be fulfilled. First our calculations suggest that we will need a priori information on the speed of the object with an accuracy of approximately 7.5 m/s and the central frequency of the reception band of the optical amplifiers must match the frequency of the space-object-reflected laser pulse (based on estimate of object velocity). Second, since the moment of arrival of the reflected illumination pulse (pulse duration of 10^{-8} sec) at the receiving system depends on distance to the space object, for reflected pulse to be within the turn-on time of the optical amplifiers the distance to space object must be known to an accuracy of approximately 1.5 m. One possible range-finding concept to address this ranging requirement involves the use of a laser with 10-nanosecond pulses operating at 10 Hz or faster. Using this concept, currently we can perform a single point range measurement with an accuracy of approximately 0.75 m. With sequential pulses and the given individual range measurements, we should be able to estimate the average velocity component of the space object and also quantify the corresponding acceleration and measurement uncertainty. Nonlinear extended Kalman filtering techniques can be used to estimate the position of the space object for the next pulse, thereby further improving the illumination pointing accuracy for the next measurement. Our preliminary calculations indicate that for this approach to work, we will need to collect data for approximately 0.5 seconds to meet the velocity and range accuracy requirements. Alternatively, we could use shorter pulse lasers such as the 100-Hz picosecond ranging laser that Sandia is currently developing through an Engineering Campaign 6 project, though it may lack sufficient energy to create a measurable signal return from a rough scattering space object. Nevertheless, if it is used in conjunction with the proposed Brillouin-enhanced four-wave mixing scheme and the optical amplifier, it might be able to provide enhanced ranging accuracy once the initial detection loop is created.

Another practical challenge is associated with the sensitivity of the amplifier to scattered light. This amplifier only needs about 3 photons to engage, which is both a strength (great sensitivity) and a potential weakness (enhance noise). Though spectral filtering will limit the system response to the illumination laser signal, it may not be able to distinguish between signal reflected from the space object and signals scattered from other sources such as small debris and aerosols. Integrating the illumination laser pulse with the amplifier to provide range gating may mitigate this challenge to some extent by limiting the region in space that can contribute scattered photons to the optical receiver, but it remains to be demonstrated how robust this approach will be.

For the required distance to the space objects (150 to 1500 km) the time of double pass between the space object and the optical amplifier is 1-10 msec. During this time, the angular position of the space object will change by approximately 5×10^{-5} rad (azimuth component of space object speed is assumed to be 8 km/s) such that a phase conjugated beam may miss the space object. The direction of the phase conjugated laser radiation should be changed by a lead angle corresponding to the angular change in the position of the space object. Since the velocity and range of the space object will be measured, the lead angle can be sufficiently set using an electro-optical deflector placed in front of the input lens. The required lead accuracy (i.e., error at which the efficiency of the concentration does not worsen to any significant degree, corresponds to the resolution angle of receiving aperture). If we assume that during tracking the space object

observations will occur at a frequency of at least 10 Hz (faster is possible), then the tracking accuracy between two observation events (100 ms) is no worse than 1 arc second, resulting in a tracking error that is within 3.2×10^{-7} rad. This is less than the angular resolution of 3.6×10^{-7} rad, which corresponds to a maximum possible receiving aperture of 350 cm which is far larger than anything that would be employed. Therefore, the tracking accuracy of ~1 arc second for 0.1 seconds should be more than adequate for illumination concentration. However, it is worth noting here that the lead angle should not be more than the turbulence isoplanatic angle (the angular separation at which the atmospheric perturbations applied to the light from initial and lead angle path becomes uncorrelated) or the quality of compensation of turbulent inhomogeneities during the phase conjugated space object signal propagation through atmosphere will be reduced, inevitably affecting the efficiency of illumination concentration. Ultimately we anticipate that this will be the governing constraint that drives the system performance requirements. The isoplanatic angle defines the radius of a circle upon the sky within which atmospheric wavefront disturbances may be considered approximately uniform. To first order, the isoplanatic angle can be defined as a constant (often 0.3) times the ratio of the atmospheric coherence length to the weighted average height of the turbulence. For our applications we typically anticipate having isoplanatic angles in the range of 5 to 30 arc seconds (consistent with measurements at the Russian sites), which should be acceptable for our proposed approach.

Illumination Laser Options

Various laser options are available as laser illumination sources. Initially we had anticipated using a high-energy system consisting of Nd:glass rods with large flashlamps or laser-diode arrays pumping. However, the emergence of a new fiber laser in the summer of 2008 offers an alternative that provides good installation flexibility and improved capabilities. Further, using a fiber laser makes it easier to avoid damaging the optical elements. The Russian Sapsan concept discussed previously will include the incorporation of the IPG fiber laser as a first step, though they might replace it at a later date with a short pulse broader spectrum laser (or multiple lasers with different wavelengths) to help reduce speckle effects.

Figure 12 provides a picture of the new IPG fiber laser. This system, which can be acquired as a CW or pulsed system, currently provides 6 kW of power (IPG has near term plans to extend this to more than 10 KW). The following are a summary of the key aspects of this compact high power laser.

- Developer: IPG Laser GmbH
- Maximum power: 6 kW (now), on track for 15-20 kW by FY10.
- Wavelength: 1018 nm
- Beam quality: $M^2 < 1.2$ (measured with Primes Laser Quality Monitor)
- Measured Value $M^2 = 1.11$
- Delivery fiber: 1 m
- Modulation: up to 2 kHz
- Consumption: ~ 29-30 kW
- Wall-plug efficiency: ~ 20-21%
- Footprint: 856 × 806 mm
- Volume: ~ 1 m^3
- Power / Volume ratio: 5.9 kW/m^3

Figure 12: IPG fiber laser for illumination of space objects

Test Plan Options

The next step to evaluate the viability of proposed nonlinear methods for illuminating and imaging hypervelocity space debris involves controlled tests to demonstrate the ability to concentrate laser illumination on a test object through a turbulent medium and the ability to create a high-quality image. As a follow up to this brief study, a formal test plan will be developed and executed to quantify the performance of the proposed nonlinear techniques. As a starting point, the following two preliminary test plans have been drafted as a starting point. Many technical details still need to be addressed and these plans will certainly evolve, but these draft plans are provided herein to give some insight into the type of tests under consideration.

BEFWM Lab Test Scheme

The BEFWM test experiment will begin by reassembling the BEFWM scheme initially used by Kulagin, Pasmanik, and Shilov to investigate sensitivity, resolution, vision field and other parameters of the BEFWM image receiver [10]. The optical scheme for this experiment is presented in Fig. 13. Here, a two-pulse master oscillator will be used to provide a couple of pulses with controlled time delay between them for an initial illumination of the target area and a following pump of BEFWM. Both pulses should be amplified. The controlled time delay between pulses is to synchronize the arrival of the signal (reflected illumination from the target) and pump pulses into the BEFWM cell. The two-pulse master oscillator (scheme and output laser parameters) is presented in Fig.14.

This two-pulse master oscillator (MO) was developed for a previous BEFWM field experiment. The MO, in turn, consists of a diode-pumped continuous-wave oscillator and two flashlamp-pumped regenerative amplifiers. The four-channel signal generator is used to control the Pockel cell drivers and keep the triggering pulse jitter better than 1 ns. Further pulses go to the two-pass power amplifiers (laser rods – Nd:glass; single-pulse regime, i.e. rep. rate is 1 pulse per 5 minutes approximately). The laser-pulse energy can be amplified up to 10-20 J at the output from the power amplifiers. The magnifying telescopes used to spread the laser beams approximately 6 times on the way from the regenerative amplifiers to the input of the power amplifiers are not shown in the schemes. An SBS-cell filled with $TiCl_4$ is used as a SBS-mirror after the first pass in the illumination power amplifier (an upper amplifier channel) to provide an

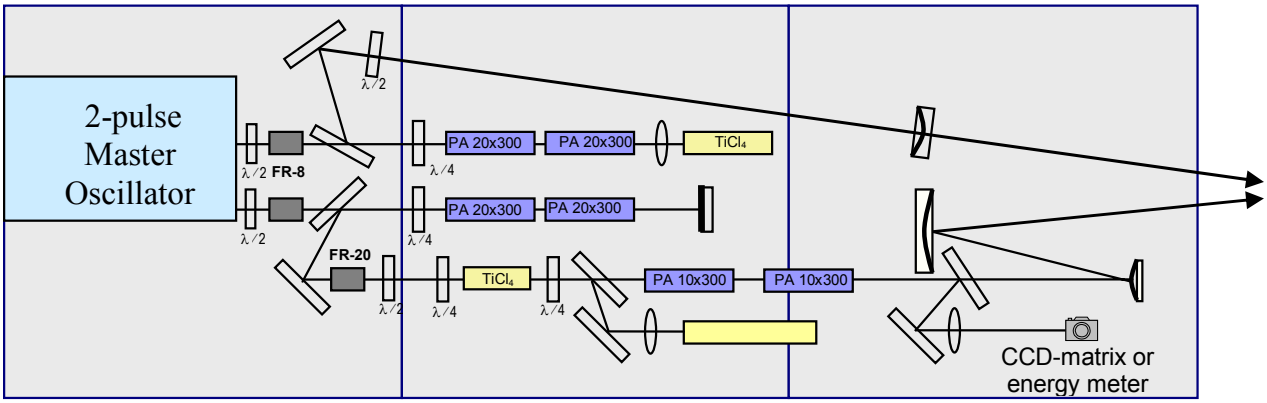

Figure 13: Proposed optical arrangement for testing of BEFWM concept for small object imaging

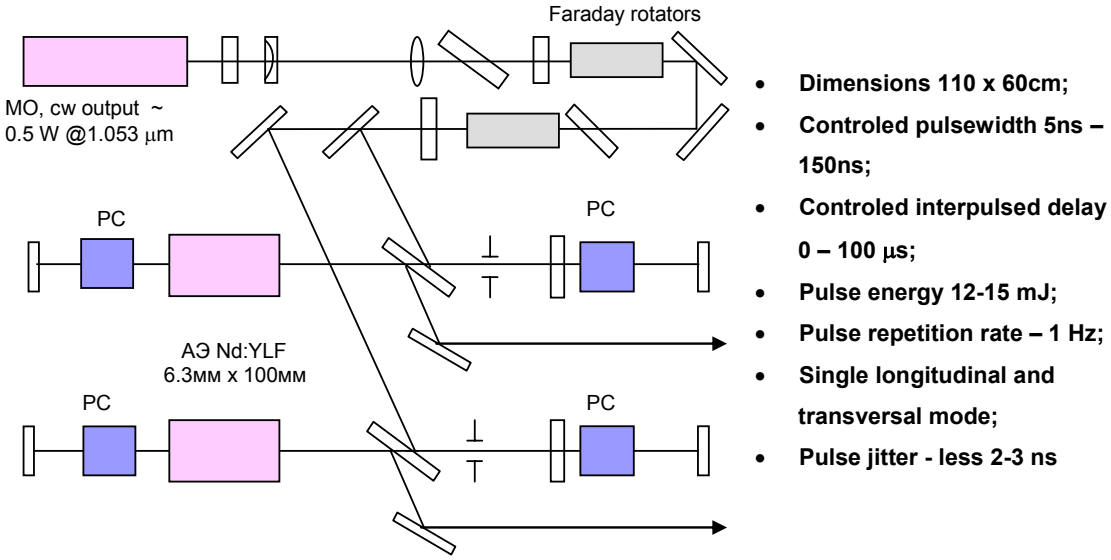

Figure 14: Schematic of two-pulse master oscillator for target illumination and BEFWM pump beams

appropriate frequency shift between the signal and pump waves at the BEFWM cell. The signal laser pulse (illumination pulse reflected from the target) is received by an input lens for further amplification in a preliminary signal amplifier. The total signal amplification before the BEFWM-cell should be more than 2000 times per pass to provide maximal input sensitivity to the BEFWM image receiver-amplifier on the level of 2-3 signal photons per pixel. As a result, the total signal energy amplification after two passes through the signal amplifiers and reflection from BEWM PC-mirror will be up to 10^{12} - 10^{14} for the weak signal. The intermediate lenses transferring the target image through the signal amplifiers are not shown here to keep the figure simple. The SBS cell filled with CCl_4 is used to arrange the second pump beam of BEFWM-cell. The total length of the laser bench in the lab is 16 m, while the BEFWM image amplifier requires a space of 4-5 m in length. Hence, it is possible to provide a distance to the target from input lens of 10 m. The facility operations and target area layout will be described below. This short-range test would be used principally as a system check out test prior to moving the test to an outdoor field-test environment with much grater target distances (hundreds of meters) from the laser setup.

In the process of equipment assembly and adjustment the following operations will be carried out:

- assemble optical elements on laser tables;
- assemble electrical units and power supplies;
- set-up adjustment;
- installation and adjustment of measurement equipment;
- determination of a power supply mode for the laser heads;
- determination of the appropriate time delays for the illumination laser and the FWHFM pump laser;
- measurement of the illumination laser and the pump laser output parameters;
- pointing of the illumination laser to the spherical reflector;
- measurement of laser energy delivered to the spherical reflector from the illumination laser;
- pointing of the BEFWM amplifier to the spherical reflector;
- measurement of the BEFWM amplifier output energy;
- measurement of the energy at the BEFWM cell input;
- measurement of the energy concentrated on the spherical reflector and the resulting beam quality.

After completing the equipment adjustments, setting the laser head flashlamp voltage levels, and establishing the time delays for the electro-optical Q-switch power supplies, the laboratory set-up should be ready for the initial concept evaluation tests. The temporal coincidence of the pump radiation and the radiation reflected off the target in the vicinity of the BEFWM cell will be checked by means of fast photodetectors and wide-band oscilloscope.

The main objective of the lab test will be to compare the energies of the radiation energy delivered to the spherical reflector, the energy of the first illumination pulse, and the energy of the second pulse concentrated after the amplifier and BEFWM reflection. Atmospheric turbulence will not naturally be present in the lab but it can be artificially generated and monitored by means of special equipment. The laboratory set-up will operate at a repetition rate up to 1 pulse per 5 minutes. For targets we will use optical glass spherical reflectors shaped as a

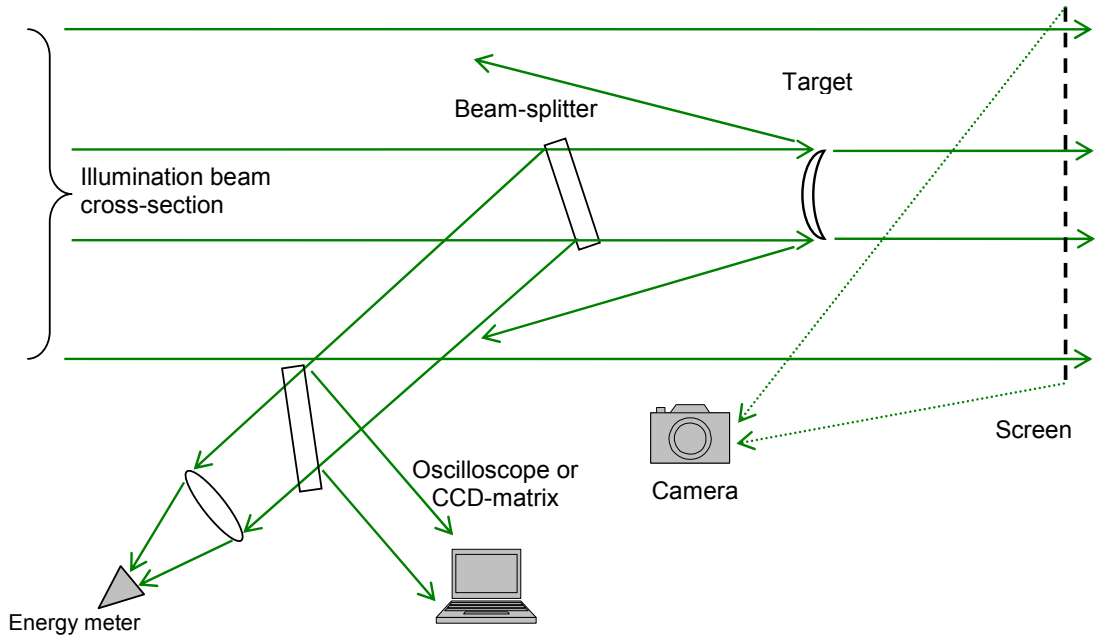

Figure 15: Target area layout for planned BEFWM experiments

uniform thickness meniscus of ~ 0.1 m curvature, the reflector diameter being ~ 0.1 m. The reflectors will be fixed in a mount minimizing illumination radiation scattering.

Special adjustment fixtures will be used during assembly as well as during the demonstration lab tests. Adjustment and pointing of the Nd:glass amplifier will be carried out by means of an auxiliary He-Ne laser or the second harmonic of an adjusting Nd:YAG laser and a sighting scope installed at the target location. During the initial adjustment phase, a retroreflector (corner cube) will be installed instead of the target to enhance reflections.

As it was stated above, spherical reflectors will be used as the initial targets. Our purpose is to show that in the target area laser pulse energy density directed to the target increases in the second pulse comparing to the first illumination pulse as a result of the application of the nonlinear optical system. That means we should acquire data regarding the laser pulse energy distribution in the target area. A possible layout of target area components is presented in Fig. 15.

Here, we need to arrange for measurements of the illumination beam parameters (i.e., a beam-splitter should be installed on the beam path). However, it is important to avoid the addition of scattered illumination from this beam-splitter or other possible sources into the signal wave (illumination reflection from the target). Hence, a minimum number of optical components will be installed in the illumination beam cross-section: the target itself in a thin mount, a beam-splitter (glass plate, AR-coated on one side and 4% reflection) for measurements from the other side, the same aperture and mount as at the target; and a wire screen behind the target with minimal scattering of the illumination wave to that can be used with a camera to capture the

initial illumination and concentrated illumination beam distribution across the all BEFWM image receiver vision field. The beam reflected off the beam-splitter will be divided for laser energy measurements and observations of the illumination pulses and their beam shape by an oscilloscope and WincamD CCD-matrix correspondingly.

This initial test will have an objective to demonstrate the capabilities of the BEFWM scheme to compensate for the phase turbulent distortions and to concentrate the returning illumination energy on the reflecting areas of the target with resolution limited by the receiving lens aperture of the BEFWM image amplifier. Therefore, we will measure the angular distribution of the initial and secondary target illumination such that their comparison will show the efficiency of laser energy concentration on the target. As a follow on, we will install the thin wire screen behind the target to observe the total distribution of laser energy in BEFWM field of vision. It should be noticed here that the distances between the target and the beam-splitter or the screen should be about 2-3 m or more to suppress the BEFWM amplification of these signals in comparison to amplification of signal from the target because of a time mismatch of an undesired signal relatively to the pump pulse in the BEFWM cell.

The BEFWM test experiments will be carried out step by step and the target area distance from the laser scheme will increase correspondingly. As tentatively planned, these initial tests will consist of four stages. In the first step, our experiments will begin in the laboratory with a target distance near 10 m. Later it will be moved to an outdoor test range. For the second step we will move the target area to the roof of adjoining building to increase the distance up to 60-70 m. The third step means moving to the neighbor roof and distance extension to the level of up to 100 m. And the fourth step is transition to the more distant roof and path from BEFWM setup to the target near 400 - 500 m. As needed, a transparent phase-distorting screens will be inserted between the illumination and signal beams to imitate the influence of strong turbulence.

Test Plan for One-pass Aberration Correction by BEFWM

As an introduction, let us consider the basic principles of our approach. Using phase conjugation one can create an efficient delivery of laser energy through optically inhomogeneous medium though compensation of the distortions associated with atmospheric turbulence and other inhomogeneities.

One of the most attractive techniques to get a conjugated wave involves the phase conjugation (PC) created using Brillouin enhanced four-wave mixing on hyper-sound. Our project is based on results from the investigation of various schemes of phase conjugation by BEFWM and amplification of optical signals tested by the Russian Academy of Sciences Institute of Applied Physics. A scheme developed for phase conjugation and optical image amplification via BEFWM is presented in Fig. 16 [13]. Here, a signal wave (green arrows) to be conjugated interacts with two powerful pump waves (red arrows). An advantage of this technique is the possibility to conjugate a weak signal wave with a reflection coefficient of more than 10^6-10^7 (i.e., amplification due to pump-wave energy conversion into conjugated signal takes place).

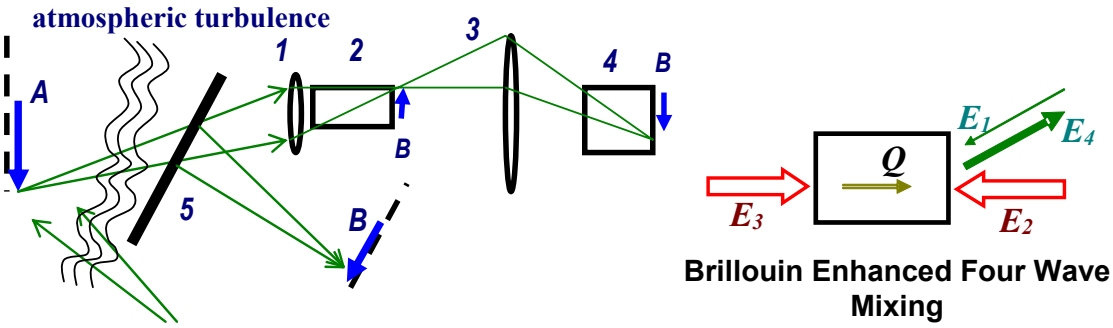

Figure 16: BEFWM image amplifier. Here: 1- input lens; 2 - laser amplifier; 3 - PC-mirror lens; 4 - PC-mirror via BEFWM; 5 - beam-splitting mirror; A - object plane; B - image plane

This set-up incorporates an auxiliary laser illuminating a target. A portion of the illumination signal reflected off the target enters a primary input lens, passes to an amplifier, and goes to a phase conjugation device. The wave conjugated in this device is amplified once again using the stored laser energy. At the same time during the second pass, distortions linked with both amplifier/optical components inhomogeneities and atmospheric inhomogeneities are compensated automatically. As a result, the laser output delivered to the target is free from distortions caused by the laser/atmosphere path/target system. A critical condition for the described laser set-up is to ensure the location of the target illuminated by the auxiliary laser is within the field of view of the amplifier/phase conjugating mirror system, while the powerful laser output focusing at the target is carried out automatically, thus providing the auto-pointing and auto-focusing of laser radiation at the target.

It is possible to create a target image in a powerful laser beam by means of PC via BEFWM with resolution limited by the input\output lens aperture. *But it will be created at the target area only (i.e., behind the distortion flow).* However we are interested in getting a high-quality target image near our laser setup, with only a single pass through the BEFWM optical phase conjugation scheme. To accomplish this some modification of the scheme in Fig. 16 is required. The idea is based on four-wave mixing implementation of real-time holography [14].

The key elements of our modified version of this scheme are the following (see Fig. 17):

- We put the corner cube in the target area (as close to the target as possible) to provide an additional reflected wave distorted by turbulence (we will need an additional illumination wave also (red arrows));
- this added illuminaton wave will be amplified, phase-conjugated in an SBS-cell, and used as a pump beam to interfere in a BEFWM-cell with the signal beam reflected off the target.
- as a result, both waves carry similar turbulent phase distortions, so distortions will be compensated in the resulting nonlinear polarization (hypersound) wave.

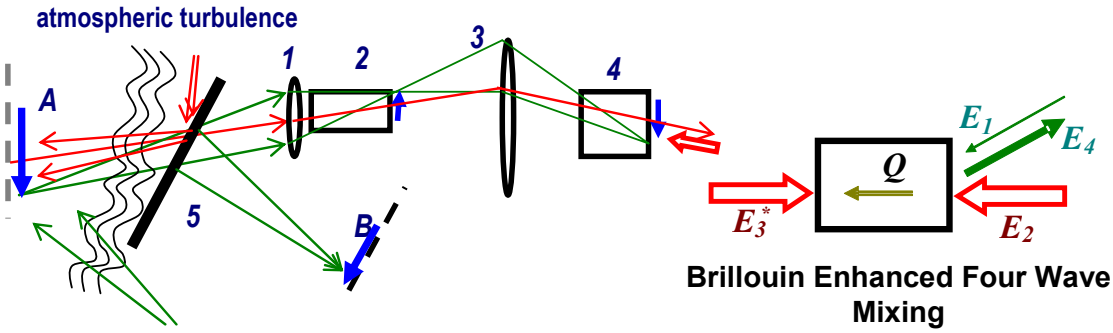

Figure 17: Idea of possible scheme modification for one-pass aberration correction. Here: 1- input lens; 2 - laser amplifier; 3 - PC-mirror lens; 4 - PC-mirror via BEFWM; 5 - beam-splitting mirror; 6 - retro-reflector; A - object plane; B - image plane

When we arrange the reflection of the second pump wave with a plane and smooth wavefront from this polarization wave in the BEFWM-cell, this reflected wave will give us a target image without turbulent phase distortions.

Considering that this concept may not be simple to understand, and further explanation of this approach is warranted (see Fig. 17 with the more detailed BEFWM scheme modified for one-pass correction). Here we add another preliminary amplifier for the reflected (by corner cube) pump wave E_3 on its way to the BEFWM cell. First one of the initially plane pump waves E_3 and a signal wave $E_1(\rho)$ reflected from the target pass through distorting (turbulent) medium. This means that pump wave E_3 is created by reflection of the illumination wave from the corner cube. If the corner cube cross-section is small compared to the resolution angle of our input lens, we can say that the turbulent distortions of the illumination wave passing to the corner cube are not important. This means we have a perfect point source behind the distorting layer. Passing through this medium, each of two incident optical fields acquires the same non-uniform phase shift (i.e., we have two complex fields on the BEFWM cell input):

$$\boldsymbol{E}_1(\rho)=E_1(\rho)\exp(i\varphi(\rho)) \qquad (2)$$

$$\boldsymbol{E}_3(\rho)=E_3\exp(i\varphi(\rho)); \qquad (3)$$

here ρ - is a transverse coordinate relative to optical axe.

A separation of waves $\boldsymbol{E}_1$ and $\boldsymbol{E}_3$ at the input of the BEFWM cell is possible using opposite polarizations in each of their illuminations.

The second pump wave $\boldsymbol{E}_2$ remains plane. To achieve the appropriate interaction of the signal wave $\boldsymbol{E}_1(\rho)$ and proper pump wave $\boldsymbol{E}_3(\rho)$, we have to provide the phase conjugation of $\boldsymbol{E}_3(\rho)$ by its focusing to the SBS cell behind the BEFWM cell (this is a traditional geometry for a

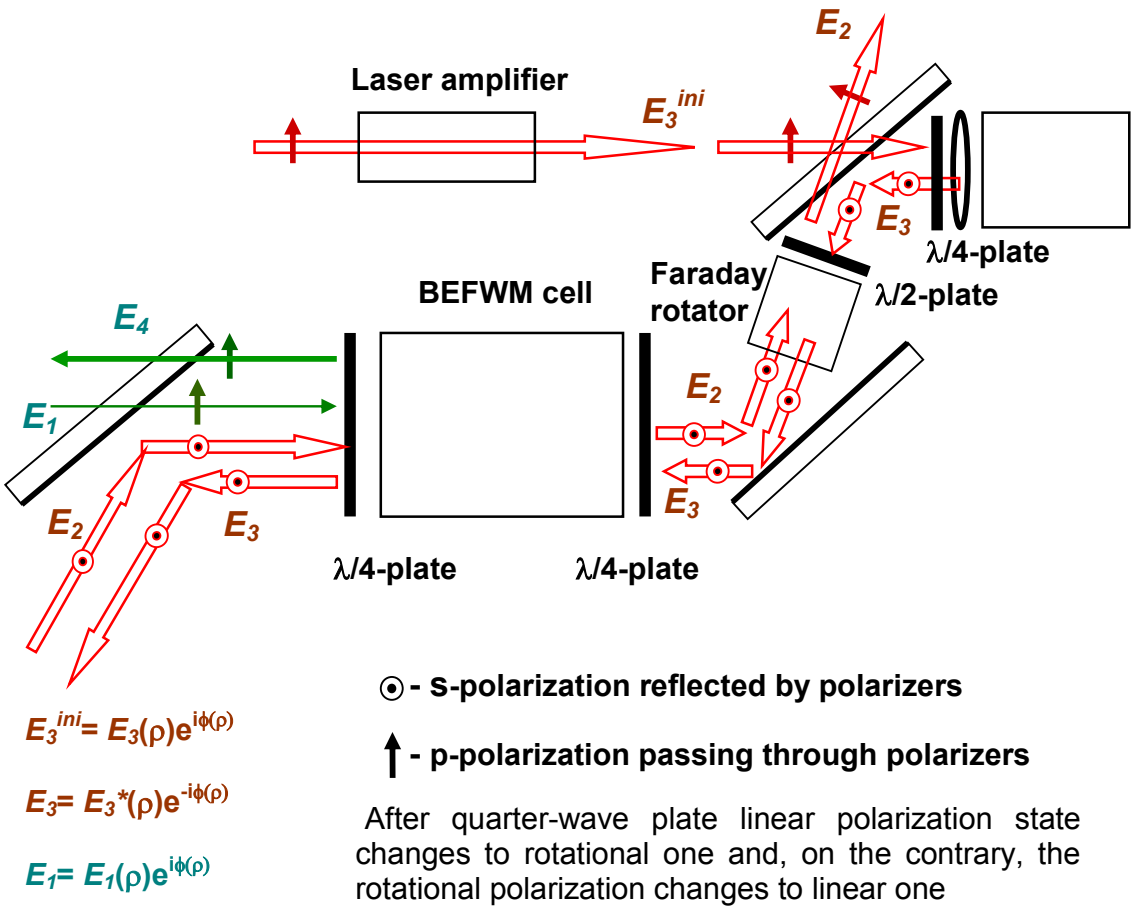

Figure 18: Modified BEFWM scheme for one-pass aberration correction

BEFWM layout). Then the conjugated wave $\boldsymbol{E_3}^*(\rho) = E_3^* exp(-i\varphi(\rho))$ is directed to the BEFWM cell. As a result, the image-carrying signal and reference waves in the nonlinear medium of the BEFWM cell contains information about turbulent distortions in identical exponentials phase factors and. their nonlinear interaction in the BEFWM medium will result in autocompensation for turbulence and other distortions in the E_1 and E_3 waves in the third-order nonlinear polarization induced in the BEFWM medium:

$$P_{NL} \sim E_1^*(\rho) exp(i\varphi(\rho))\, E_3^* exp(-i\varphi(\rho)) \quad (4)$$

$$E_2 = E_1^*(\rho)\, E_3^*\, E_2 \quad (5)$$

Thus, the wave generated by the non-linear polarization is free of distorting effects $E_4 \sim E_1^*(\rho)$.

A schematic layout of the BEFWM image amplifier for experimental testing of the one-way phase distortion correction is shown in Fig. 18. An additional preliminary pump amplifier channel is seeded by reflection of part (near 30%) of the amplified BEFWM pump beam. This beam after further amplification is directed to the corner cube at the target area. Then the

returning reflected pump beam passes to the SBS-cell filled with CCl_4 due to a polarization state change caused by the double pass through a quarter-wave plate. This conjugated beam will be used as a BEFWM pump beam $\boldsymbol{E}_3(\rho)$. As one can see, we have to install some additional components. In particular, an additional laser head, the second 20-mm Faraday rotator to provide extraction of the pump beam from the scheme after BEFWM-cell pass and an additional SBS-cell filled with CCl_4 to provide an appropriate connection of interacting wave frequencies at BEFWM are required

The phase correction efficiency will be checked by measurements of the target image quality in the conjugated and amplified output signal beam E_4 using a CCD-matrix (see Fig. 18). The additional aberrators (phase distorters) will be installed along the path of the signal and pump illumination beams to imitate an influence of turbulent flow. We plan to implement this modified scheme modification and test this approach experimentally during the laboratory stage of BEFWM tests after completing the restoration of the BEFWM technique and first lab tests of the scheme presented in Fig. 2.

Conclusions

Multiple ground to space telescope systems are under development in the United States and Russia to improve ground to space imaging capabilities. Unfortunately most of these efforts are pursuing improved designs that follow relatively conventional approaches. One exception it the Russian work involving the use of nonlinear optical methods for providing high quality space object illumination, focused lighting to induce glints for use with adaptive optics systems, and for improved imaging using phase conjugation. As a follow on to this study, variants of the test plans presented in this report will be conducted in calendar year 2009 to demonstrate proof of concepts for the nonlinear optical techniques for imaging and laser propagation through atmospheric turbulence.

Acknowledgements

Many of the concepts discussed in this report were developed in partnership with Dr. Alexander Sergeev (Russian Academy of Sciences Institute of Applied Physics, RAS-IAP) Dr. Oleg Kulagin (RAS-AIP), and Professor Victor Shargorodskiy (Russian Space Agency's Science Research Institute for Precision Instrument Engineering, FSUE-IPIE). The authors would like to acknowledge their participation and contributions to this study.

References

1. L.V. Rykhlova. “Contamination of the vicinity of the Earth by space debris,” *Proceedings of “Near-Earth Astronomy-2003”*, vol. 2, pp 11-19, Terskol, September 813, 2003.

2. J. Williamsen, “Satellite Vulnerability to Direct Ascent KE ASAT: Applying Lessons Learned from NASA, Missile Defense, and Aircraft Survivability Programs,” Aircraft Survivability, Summer 2008.

3. Editorial: “The Growing Orbital Junkyard,” *Space News Business Report,* 15 August, 2006, http://www.space.com/spacenews/archive06/Editorial_0814.html

4. S. Silva *et al*. “Eliminating Space Debris,” Applied Technology and Policy Prescriptions, USSTRATCOM Global Innovation and Strategy Center Project 07-02, January 2008.

5. D. Mehrholz *et al.,* “Detecting, Tracking and Imaging Space Debris,” ESA bulletin 109 — February 2002.

6. J.W. Campbell, “Using Lasers in Space, Laser Orbital Debris Removal and Asteroid Deflection,” Occasional Paper No. 20, Center for Strategy and Technology, Air War College, Air University, Maxwell Air Force Base, December 2000.

7. A. Gorman, “The Archaeology of Orbital Space,” *Australian Space Science Conference*, pp. 338-357, RMIT University, Melbourne, 2005.

8. C. R. Phipps, “ORION: Clearing near-Earth space debris in two years using a 30-kW repetitively-pulsed laser,” http://www.seds.org/archive/spaceviews/9707/articles.html#1

9. T. Reichhardt, “Satellite Smashers, Space-faring nations: clean up low Earth orbit or you're grounded,” *Air & Space Magazine*, March 01, 2008.

10. O.V. Kulagin, G.A. Pasmanik, and A.A. Shilov, “Amplification and optical phase conjugation of small signals,” *Uspekhi Fizicheskih Nauk*, v.162, pp. 129-157, 1992.

11. *Phase Conjugate Laser Optics*, A. Brignon and J. Huignard, eds, Wiley, 2004.

12. O.V. Kulagin, personal communication, July, 2008.

13. O.V. Kulagin, G.A. Pasmanik, and A.A.Shilov "Amplification and phase conjugation of weak signals," *Soviet Physics Uspekhi,* vol. 35, pp. 506-519. June 1992.

14. K.R. MacDonald, W.R. Tompkin, and R.W. Boyd, "Passive one-way aberration correction using four-wave mixing," *Optics Letters*, vol.13, p.485-487, 1988.

Distribution

1	MS	0549	R.A. Neiser, 5918
1		0826	S.P. Kearney, 1512
1		0826	M.T. Valley, 1512
1		1207	J.R. Yoder, 5928
1		1217	M.R. Ackermann, 5928
1		0899	Technical Library, 9536 (electronic copy)